The Experimental and Numerical Investigation of Internal Heat Transfer for Supercritical Carbon Dioxide Cooling in a Staggered Pin Fin Array and Single-Jet Impingement

Ryan Wardell*, John Richardson, Emmanuel Gabriel-Ohanu, Marcel Otto, Matthew Smith,

Erik Fernandez, Jayanta Kapat

8th International Supercritical CO2 Power Cycles • February 27 – 29, 2024 • San Antonio, TX, USA

Supported by the DOE DE-FE0031929

Center for Advanced Turbomachinery and Energy Research
Laboratory of Cycle Innovation and Optimization

OVERVIEW

1. INTRODUCTION
2. MOTIVATION AND OBJECTIVE
3. EXPERIMENTAL SETUP
4. RESULTS
5. CLOSING REMARKS

INTRODUCTION

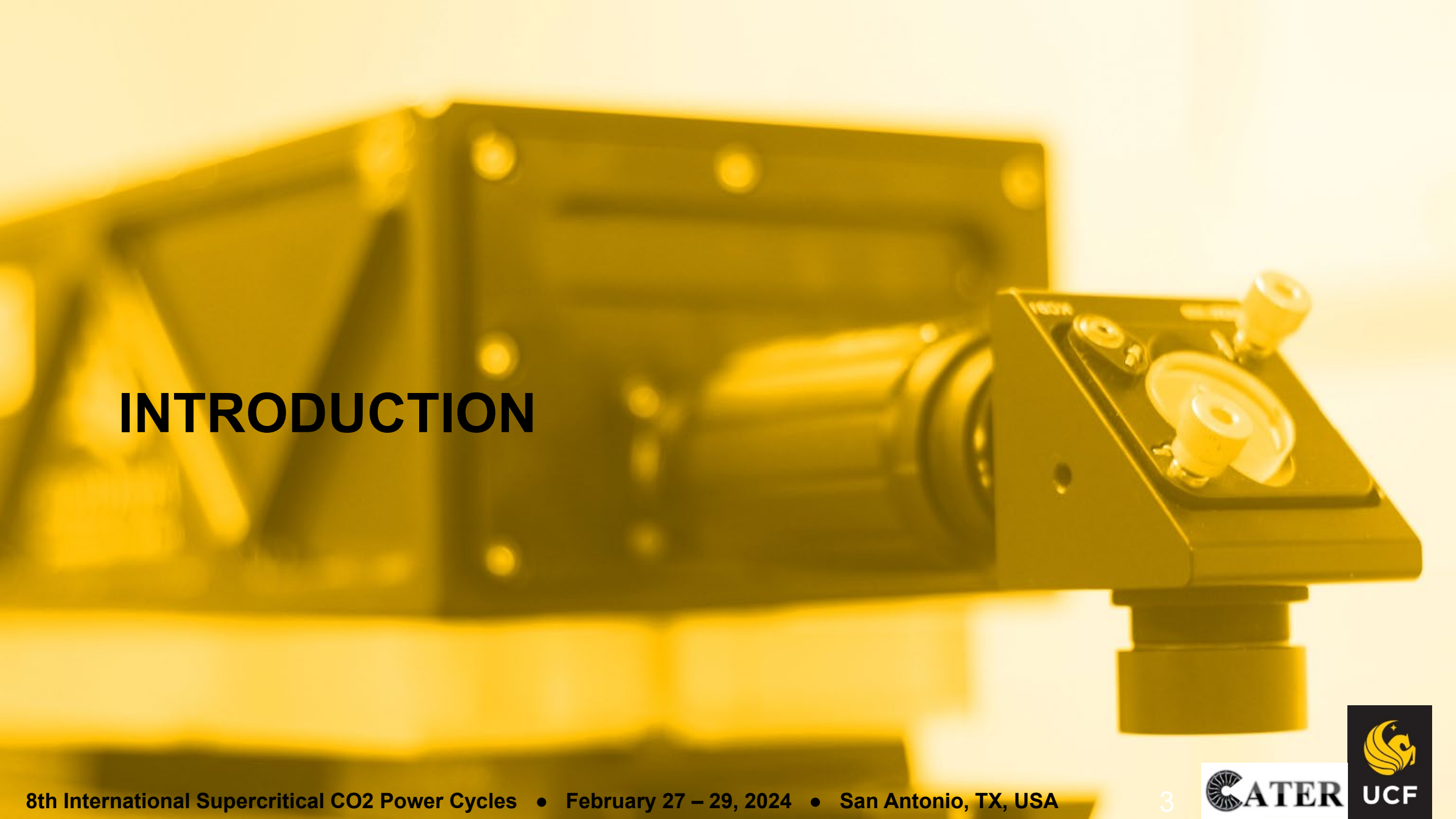

sCO_2 Power Cycle Advantages

- Supercritical carbon dioxide power cycles were found to have many advantages compared to traditional steam-Rankine and Brayton Cycles.
  - Smaller footprints due to compactness
  - Increase in thermal efficiency
  - Close to zero greenhouse gas emissions

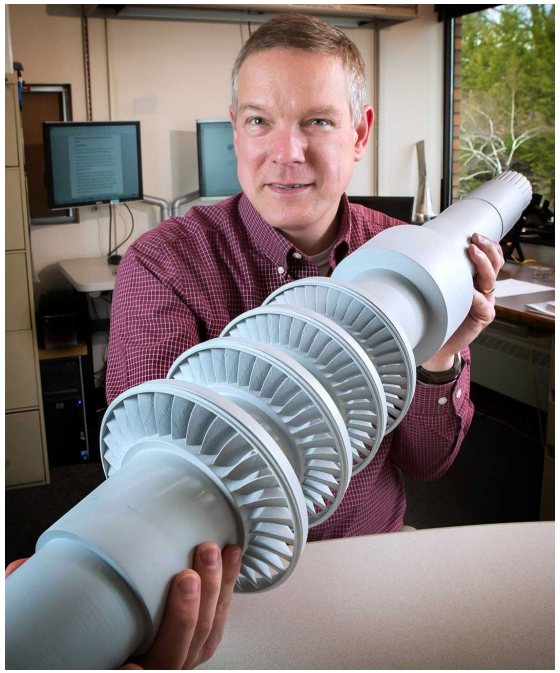

Doug Hofer carrying the desk sized 10 MWe Turbine shaft for the STEP demonstration.

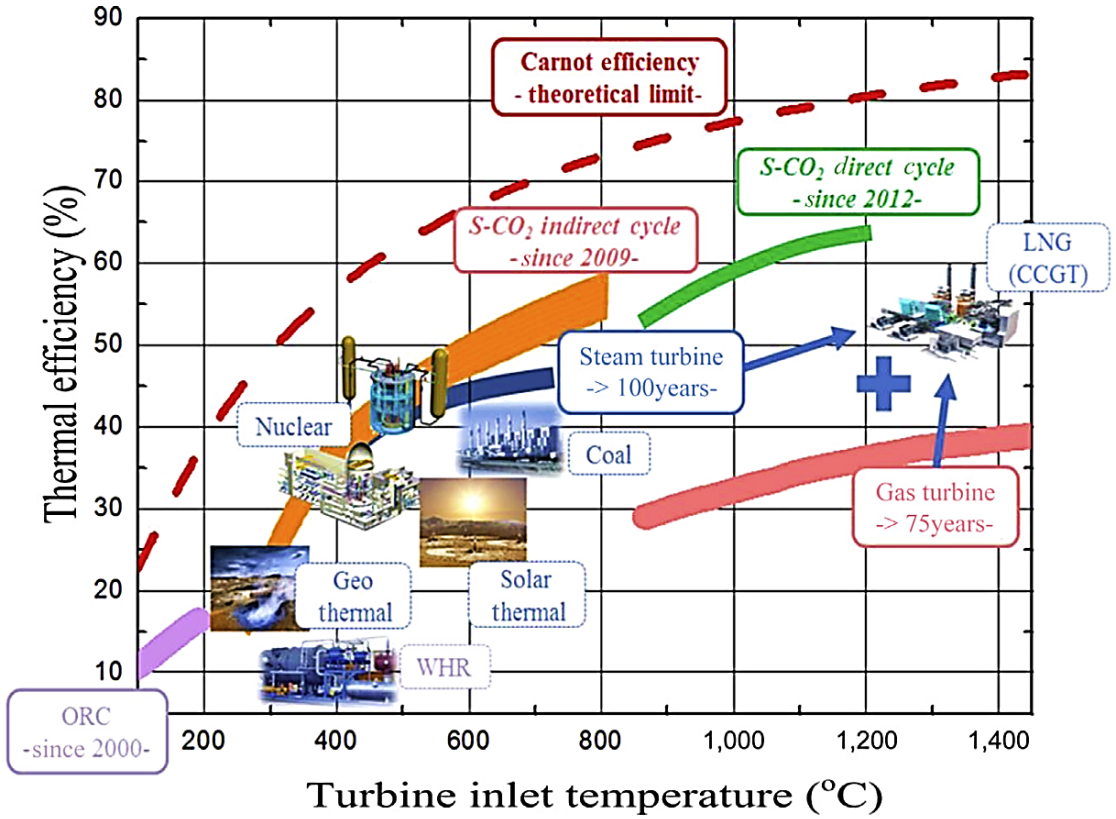

Thermal efficiencies of various power generation systems. [Ahn 2015]

Low TIT to High TIT

- STEP Pilot DEMO uses a low turbine inlet temperature (TIT)
- To transition to a high TIT, increasing thermal efficiency, need for secondary cooling.

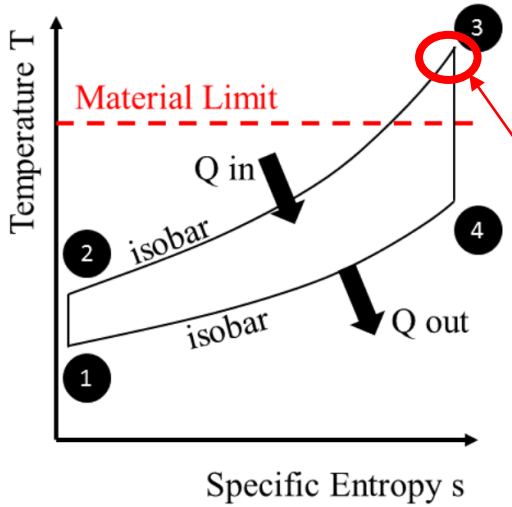

High TIT surpasses material limit. [Otto 2019]

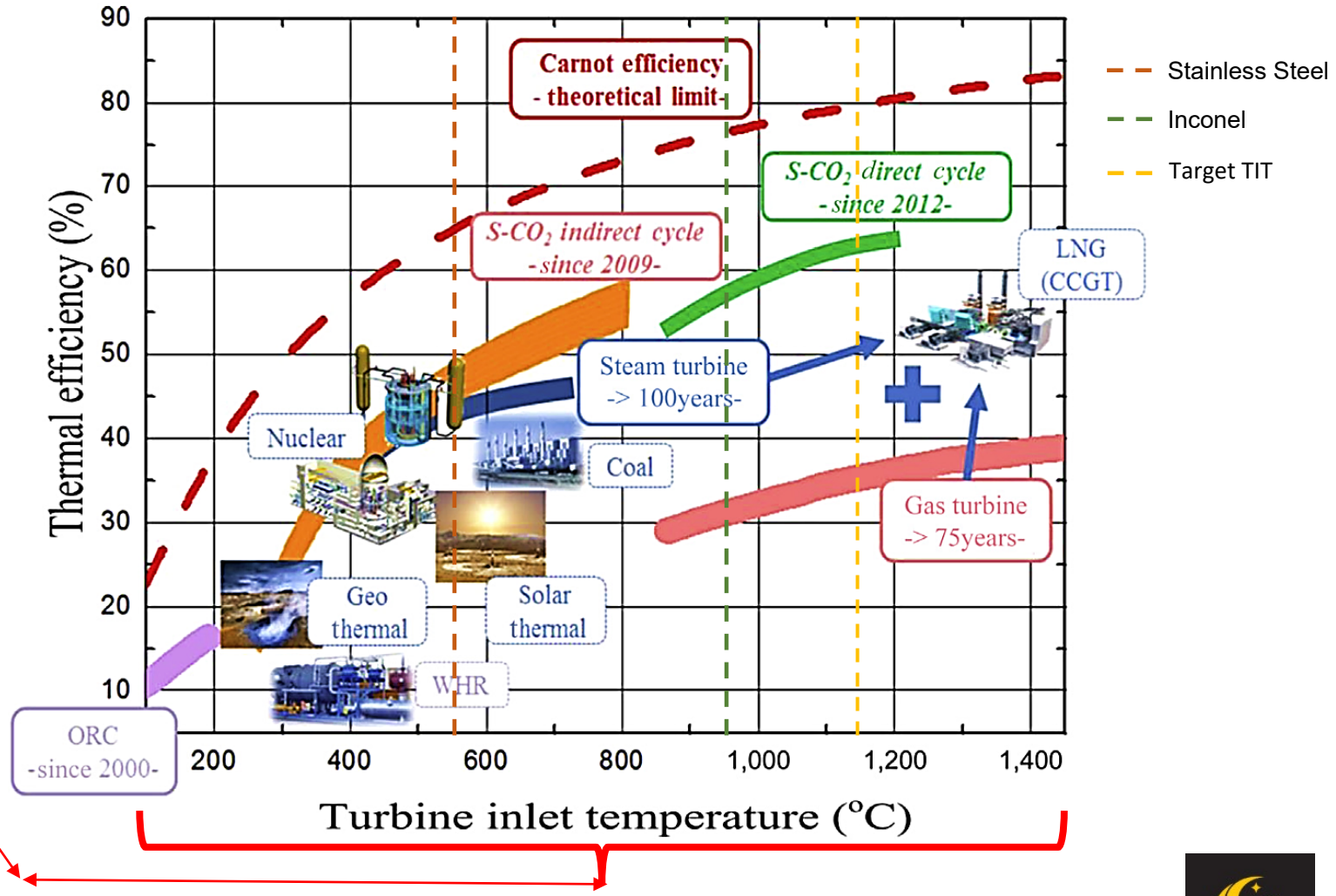

Secondary Internal Cooling in an sCO_2 Environment

- Internal cooling strategies are not new technology, with many geometric solutions having been researched in the past several decades.
- In the sCO_2 environment, however, a fundamental understanding of how these geometries impact heat transfer is lacking.
- Pin fin arrays and single-jet impingement in the trailing and leading edges of turbine blades, respectively, are two examples of secondary cooling.

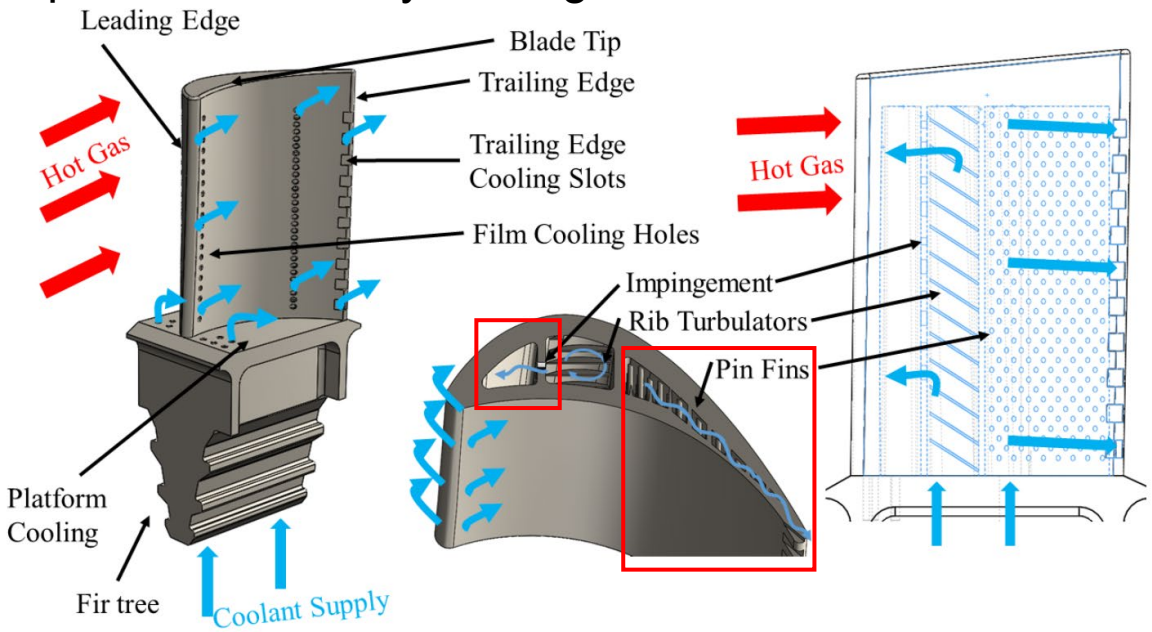

Secondary Cooling Technology in a rotating turbine blade. [Otto 2019]

Past Pin Fin Research

- Pin fin arrays are not a novel heat transfer solution.
- Pressure loss, heat transfer, pin shape, array layouts, etc. have all been topics of interest for pin fin geometries.
  - Metzger and Haley studied heat transfer with conducting and non-conducting pins. [1982]
  - Chyu studied pressure loss in inline and staggered arrays. [1990]
  - VanFossen studied how heat transfer changed in different array definitions. [1982]
  - Ames et al. studied endwall heat transfer contributions [2007] and turbulence behavior. [2005]
  - Otto studied the vortical structures in pin fin arrays [2019]

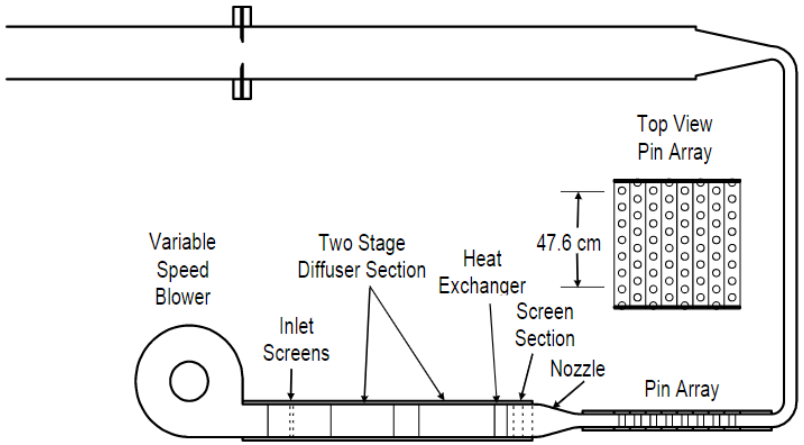

Experimental setup of Ames et al. [Ames 2007]

Pin Fin Turbulators

- Pin fin arrays are a common solution for enhancing heat transfer in the trailing edge of a turbine blade.
- Pin fin arrays serve two primary functions.
  - Act as turbulators
  - Provide structural support
- Two common orientations for pin fin arrays are inline and staggered.
- Array are defined by four dimensions. [6]
  - Pin Diameter (D)
  - Pin Height (H/D)
  - Span-wise Spacing (Z/D)
  - Stream-wise Spacing (X/D)

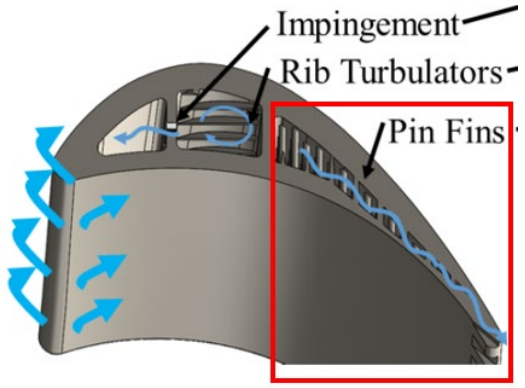

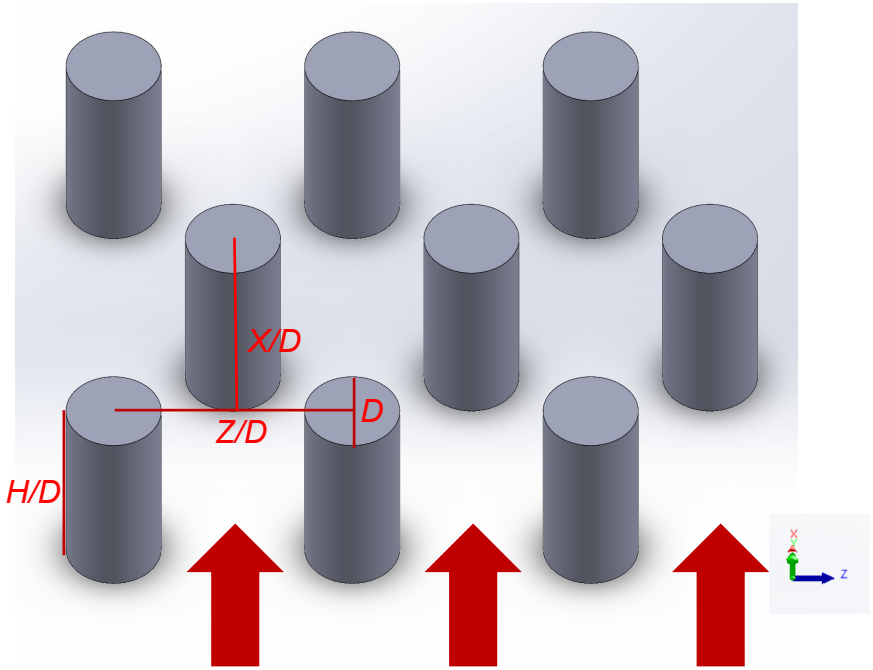

Example Pin Fin Array

Impingement Cooling

- An impinging jet is a high-velocity mass ejected from an orifice or slot that impinges on a heat transfer surface.
- Typically used in highest temperatures regions:
  - airfoil aerodynamic leading-edge regions
  - combustor liners
- Relevant parameters are mass flow, Reynolds, and Mach number; jet diameter, heat transfer coefficient, target spacing (distance from nozzle to target surface or H/D or z/D).

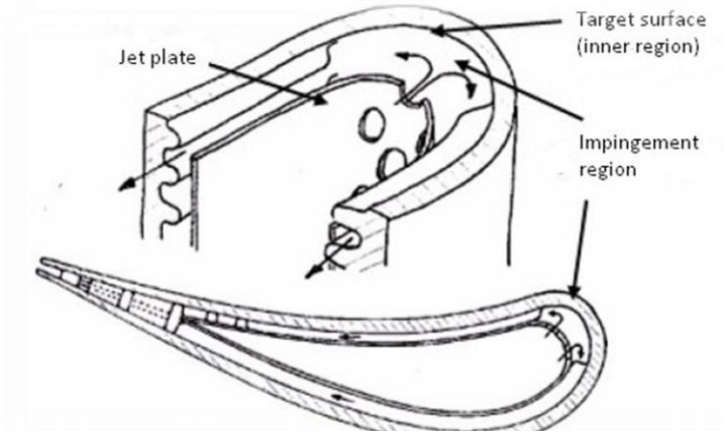

Fig. 1: Geometry for impinging flow in blade[8]

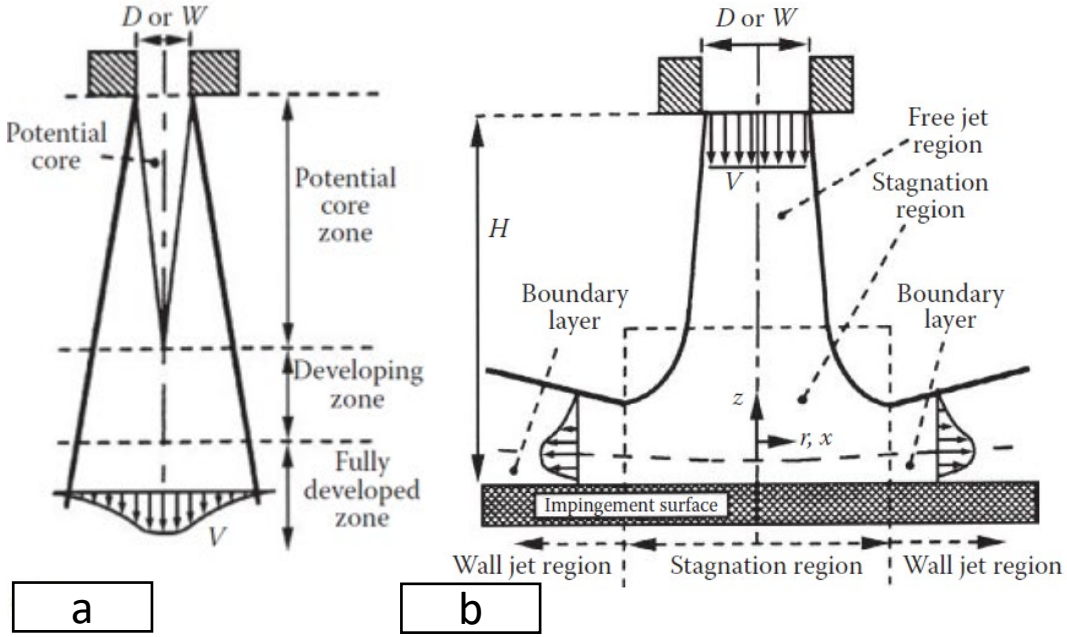

Fig. 2: Impinging jet flow profiles [Viskanta 1993]

$$h = \frac{q}{T_{wall} - T_{ref}} \quad Nu = \frac{hD}{k_f} \quad Re = \frac{\rho VD}{\mu} = \frac{4\dot{m}}{\pi D\mu}$$

MOTIVATION AND OBJECTIVE

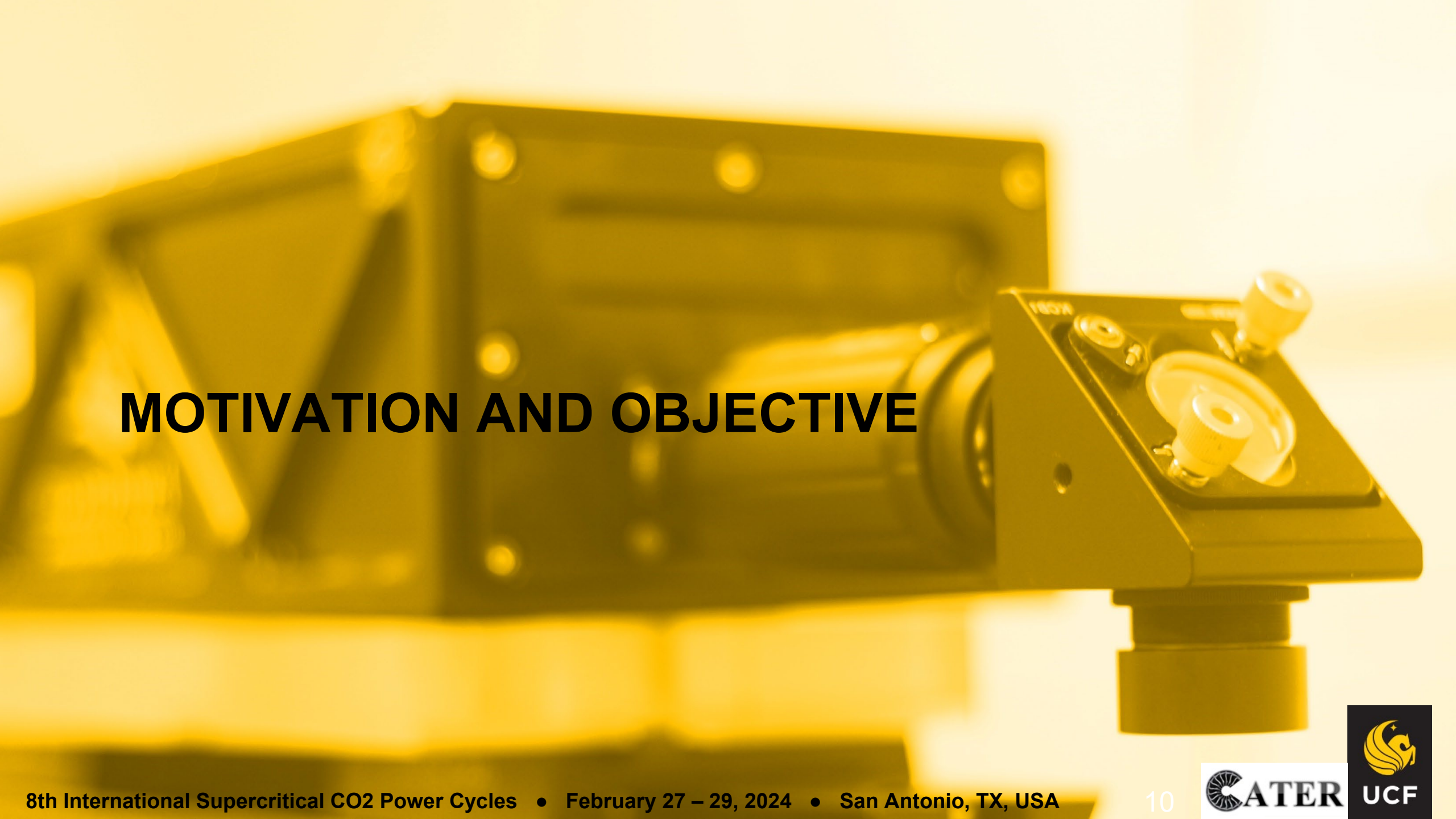

- Evolution of turbomachinery internal cooling
- However, this research was largely done with air as the operating environment, and it is unknown how this translates to the sCO_2 environment with real gas properties of the medium.
- At higher turbine inlet temperatures, internal cooling will be essential.
- Development of experimental demonstration for internal heat transfer testing at 200 bar and 400 Celsius, which sits well within the CO2 supercritical region.
- The heat transfer for pin fin turbulators and single-jet impingement in the sCO2 environment is compared to existing air data-derived correlations to quantify any deviations.
- Validating with numerical analysis

High Pressure and Temperature sCO_2 Loop at UCF

- Closed sCO_2 loop at the University of Central Florida.
- Different from UCF near critical loop that has been presented elsewhere.
- Rig Parameters:
  - 260 bar
  - 700 C (550 C for stainless steel test section)
  - 0.25 kg/s

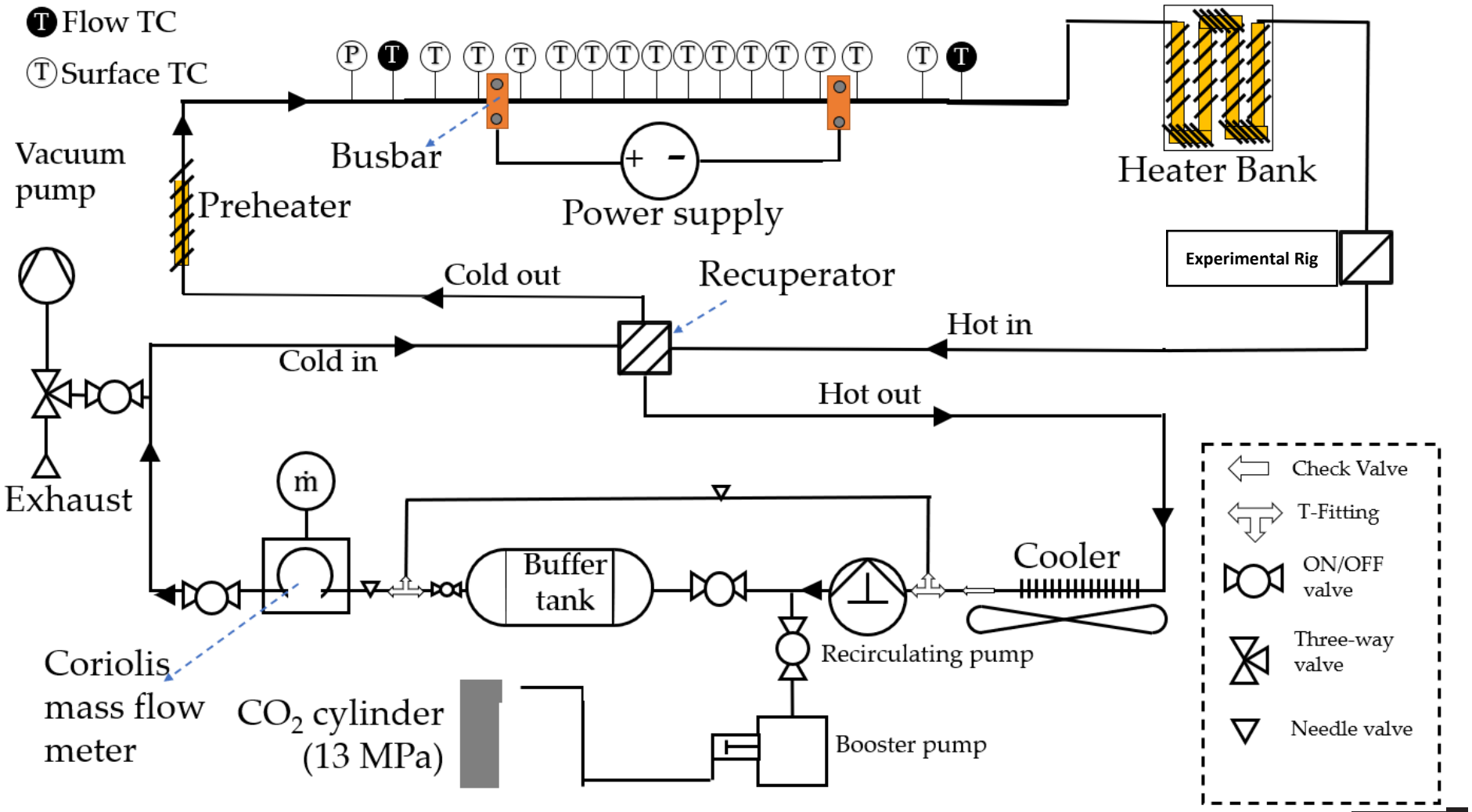

The Experimental Rigs

- The push to increase thermal efficiency means a high TIT.
- This requires secondary cooling to keep the material in operating conditions.
- CFD design allows for a fundamental understanding of the sCO_2 environment.
- Experimental Rig is designed to validate CFD with direct experimental data at operating conditions 200 bar and 400 C.

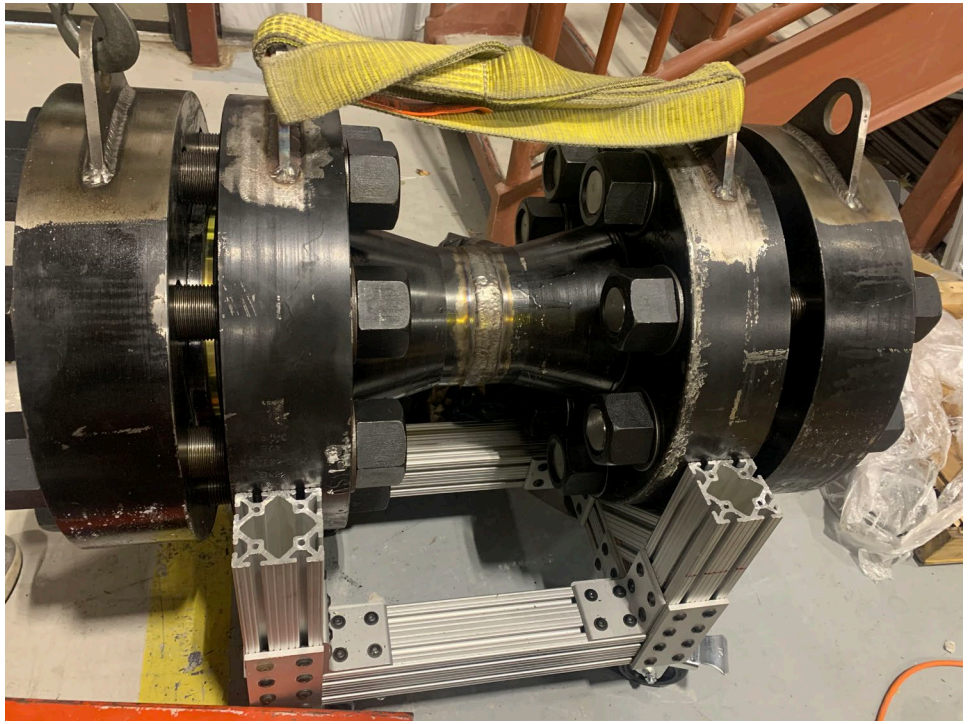

Planned Experimental Setups

PIN FIN EXPERIMENTAL SETUP

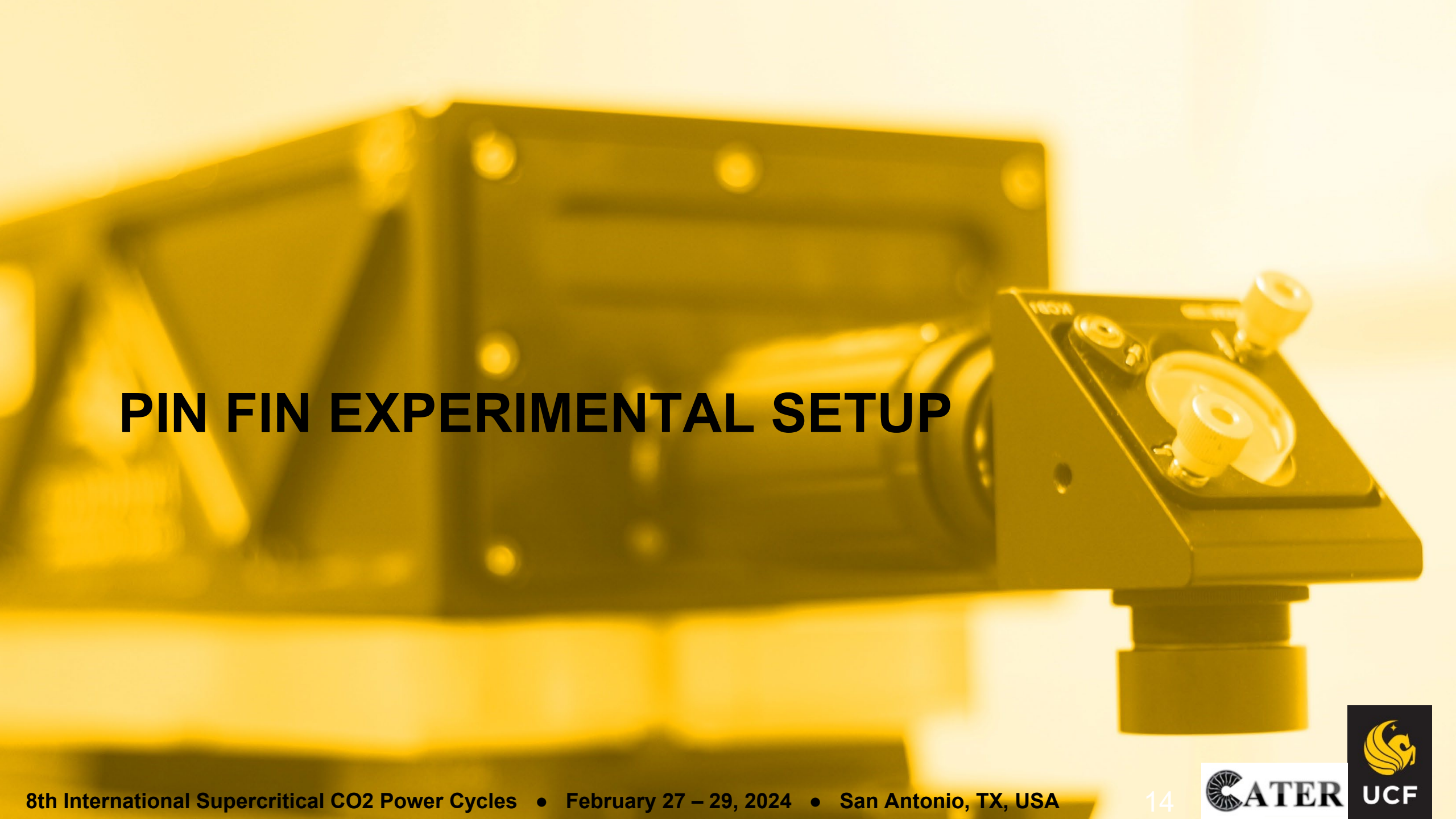

Test Section

- The pin fin test section was designed with 2mm thick side walls and 4 mm top and bottom walls.
- The parts were manufactured using CNC techniques and welded together to complete the finished test section.
- The final test section was defined by a D = 2mm and confined to a staggered 7 x 14 pin array.

Manufactured Test Section

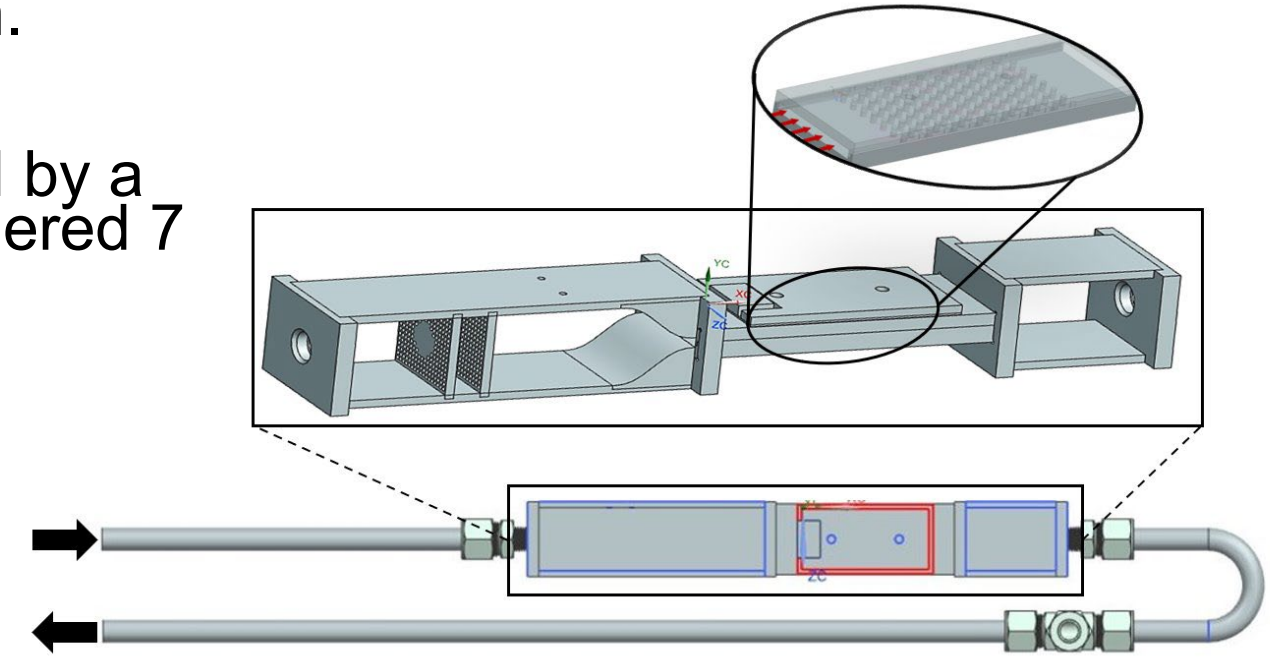

Pressure Vessel Design

- This vessel was designed by welding two 6-inch weld neck flanges and was sealed with two 6-inch blind flanges, all of which were made of carbon steel.
- This assembly weighs ~1500 lbs and was supported on an 80/20 structure to allow for mobility.
- Before integration into the loop, the complete rig was hydrostatic tested.

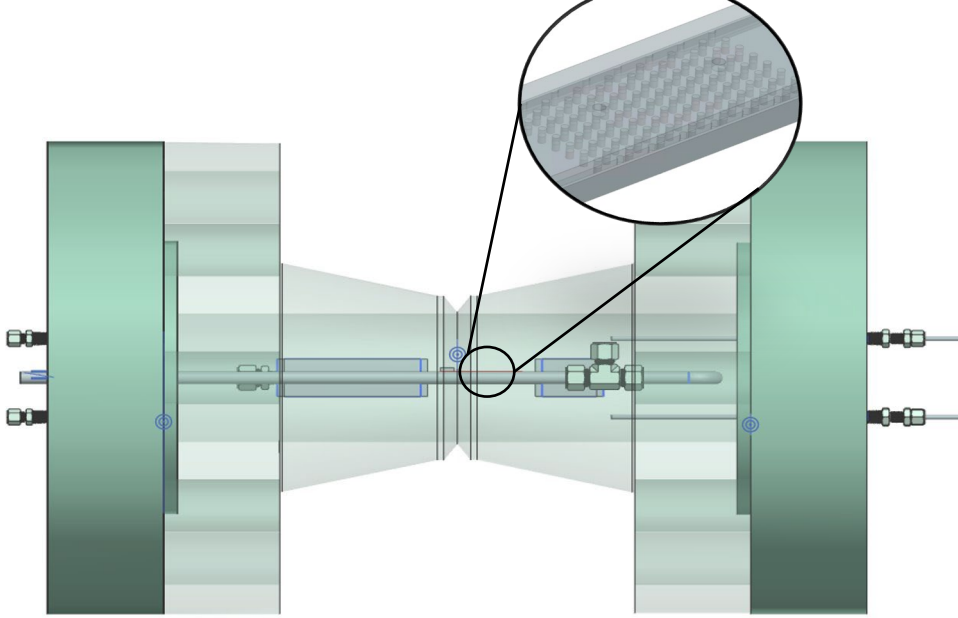

Closed Pressure Vessel

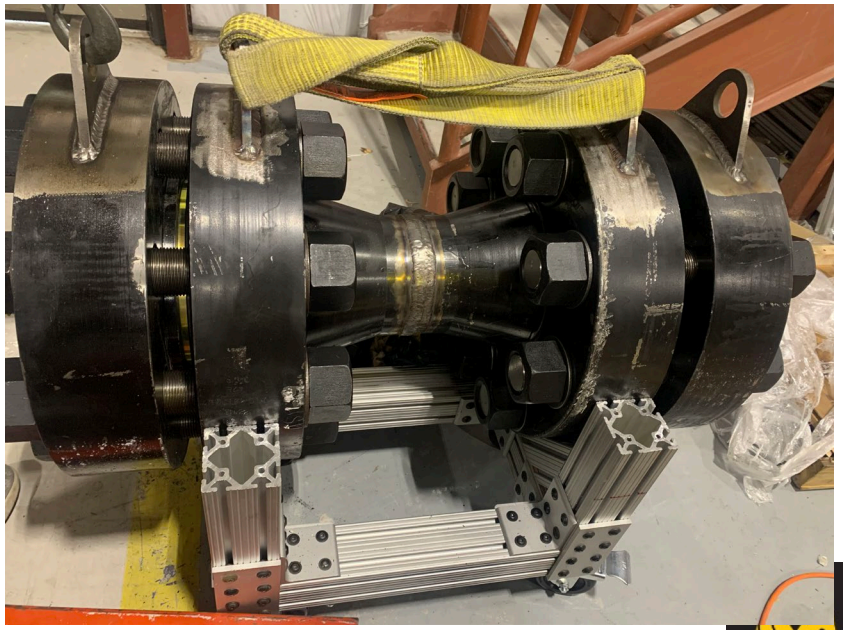

Thermocouple Placement

- The instrumentation of the loop was one of the challenges with testing at such high temperatures and pressures.
- With a limited number of thermocouple, a bulk energy balance was used to quantify the heat transfer of the rig.
- The endwall thermocouples were placed 1.5 mm form the fluid interface.
- The upstream and downstream locations for thermocouples were picked before and after the heater boundaries and positioned at the mid-line of the fluid cross-section.
- The final thermocouple was placed at the edge of the insulation to get an ambient temperature reading inside the pressure vessel.

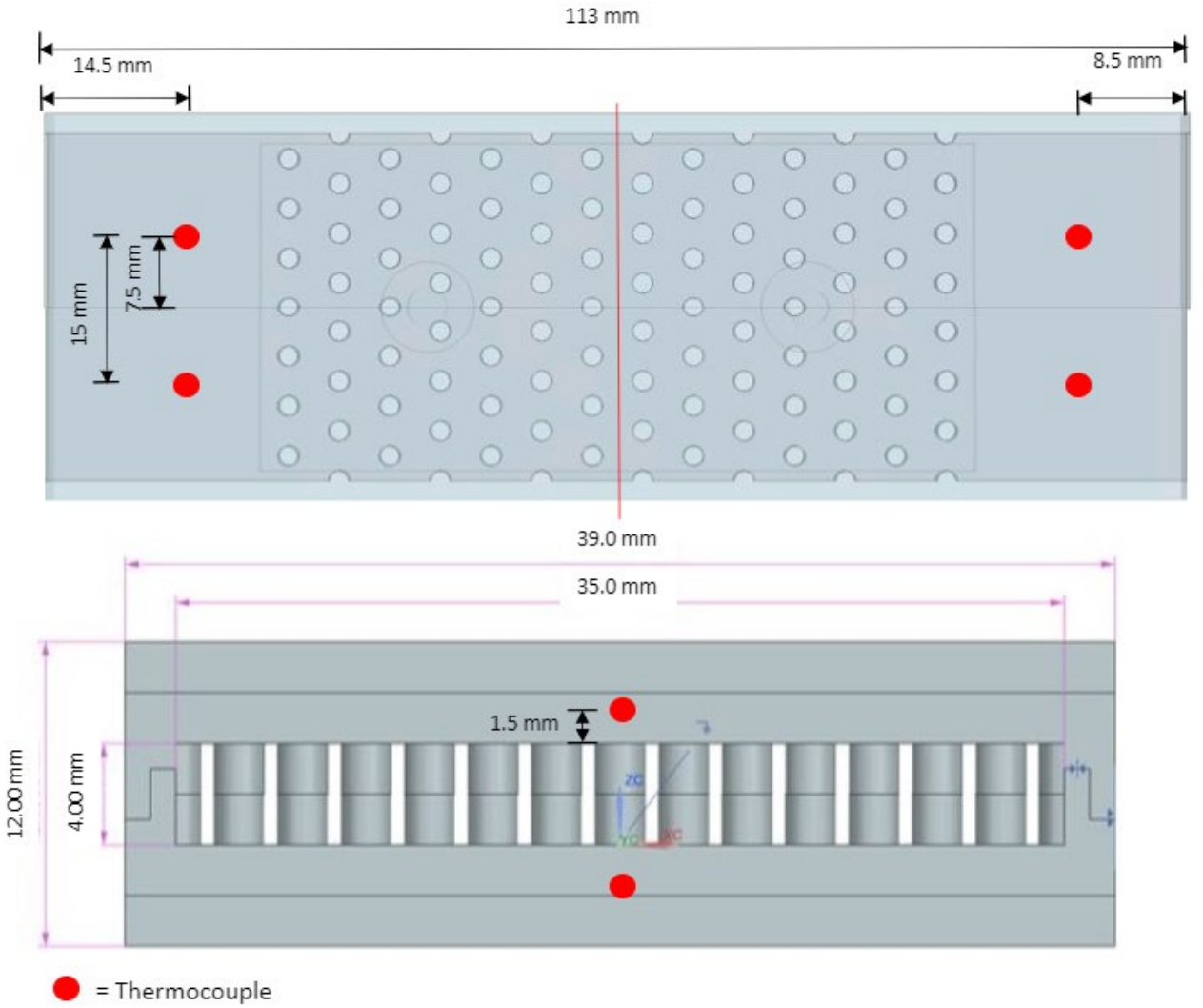

Thermocouple placement

Test Setup

- The desired testing range was from a Reynolds number of 25000 to 75000.
- For each target Reynolds number, three points were hit by varying the heat flux boundary. These were created by varying the Mica heaters.
- It was determined through testing that in this setup, the no heat flux case was the most reliable, as the heat loss within the system greatly outweighed the possible heat flux into the system due to the test section material and pressure vessel ambient environment.

Reynolds Number	Temperature (K)	Pressure (bar)	Mass Flow Rate (kg/s)
25097	679	201	0.0351
49910	679	206	0.0700
66603	675	208	0.0932

IMPINGEMENT EXPERIMENTAL SETUP

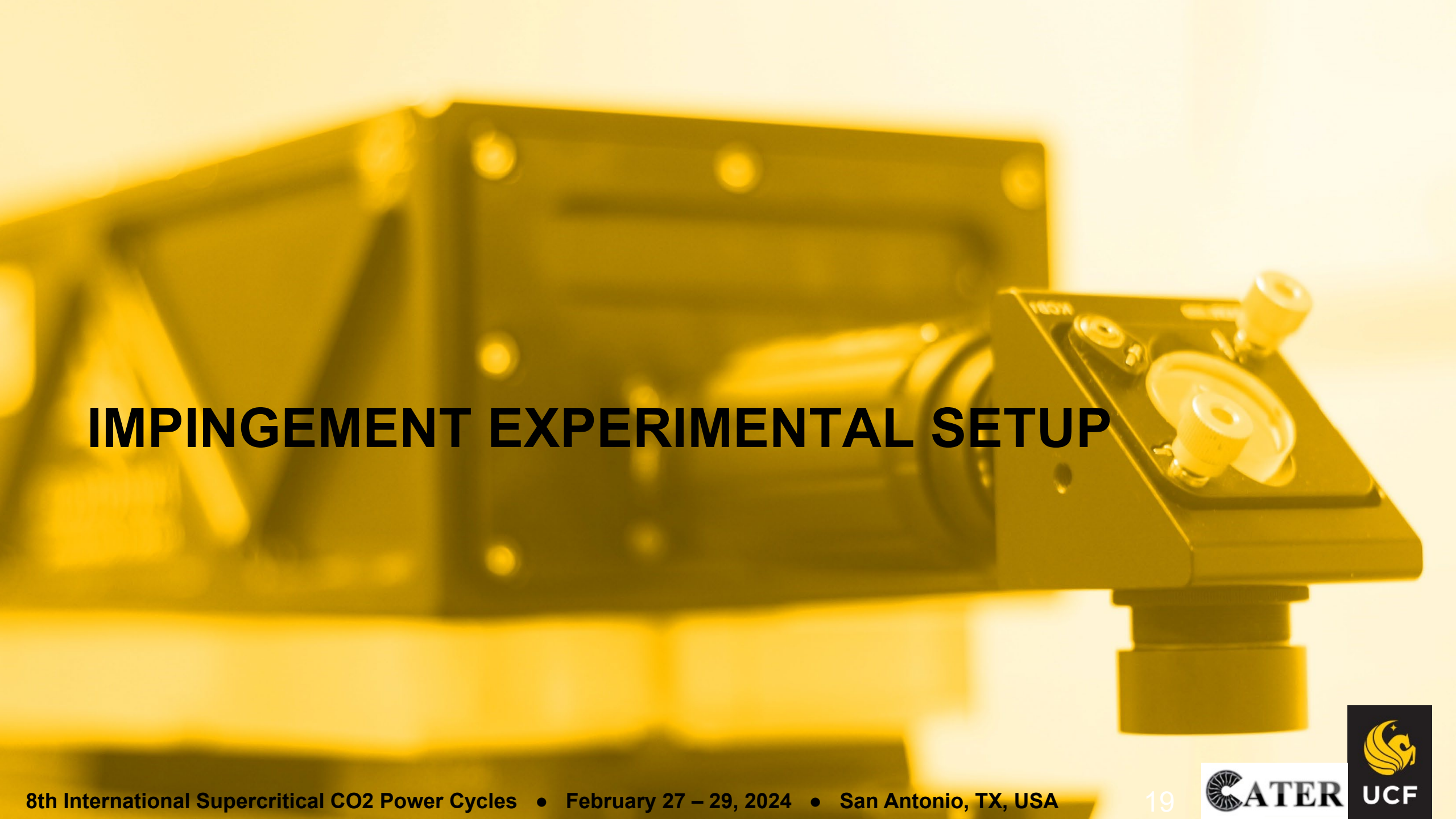

Benchtop Test Setup

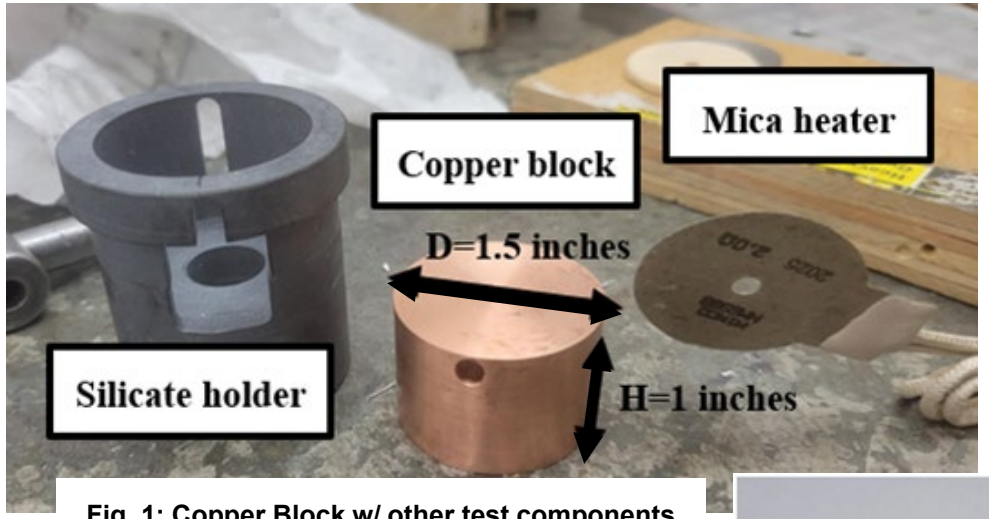

Fig. 1: Copper Block w/ other test components

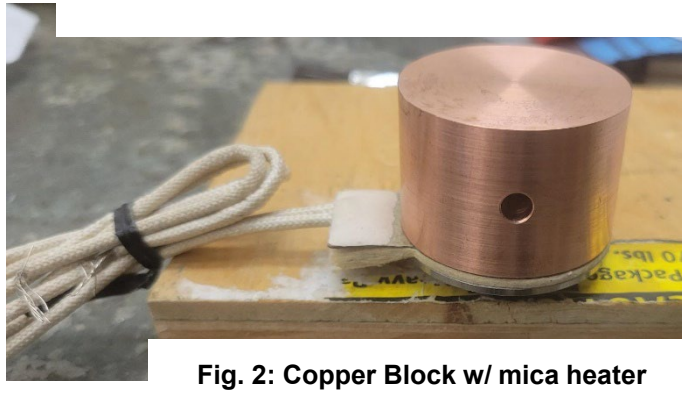

Fig. 2: Copper Block w/ mica heater

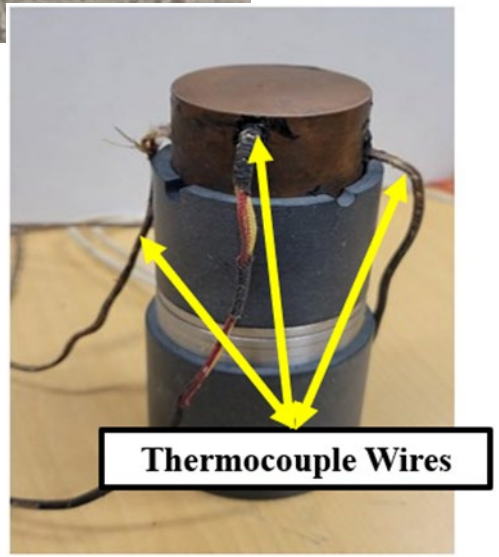

Fig. 3: Heat Transfer Setup

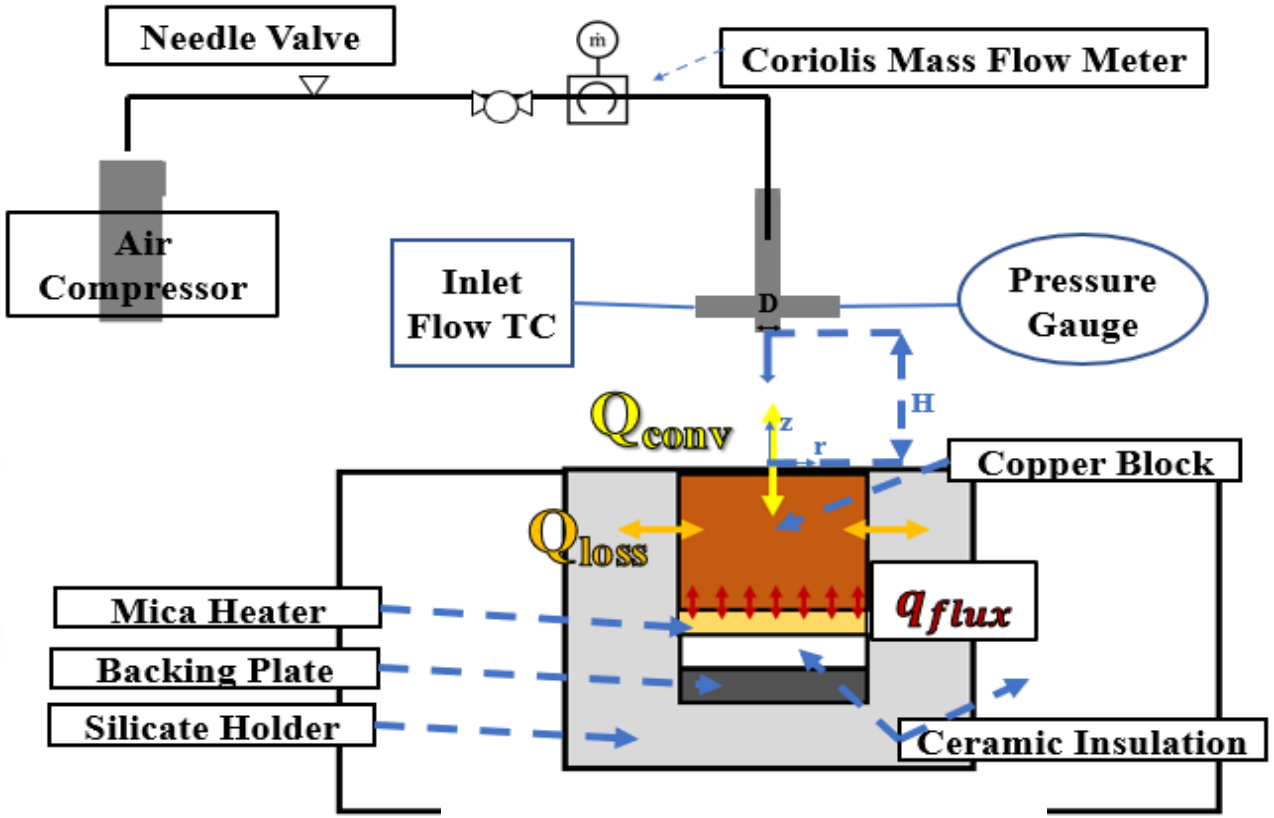

Fig. 4: Benchtop Experimental Schematic

$$Q_{flux} = Q_{convection} + Q_{loss}$$

Same components as in full experimental rig.

Air Experiments Confinement

Benchtop

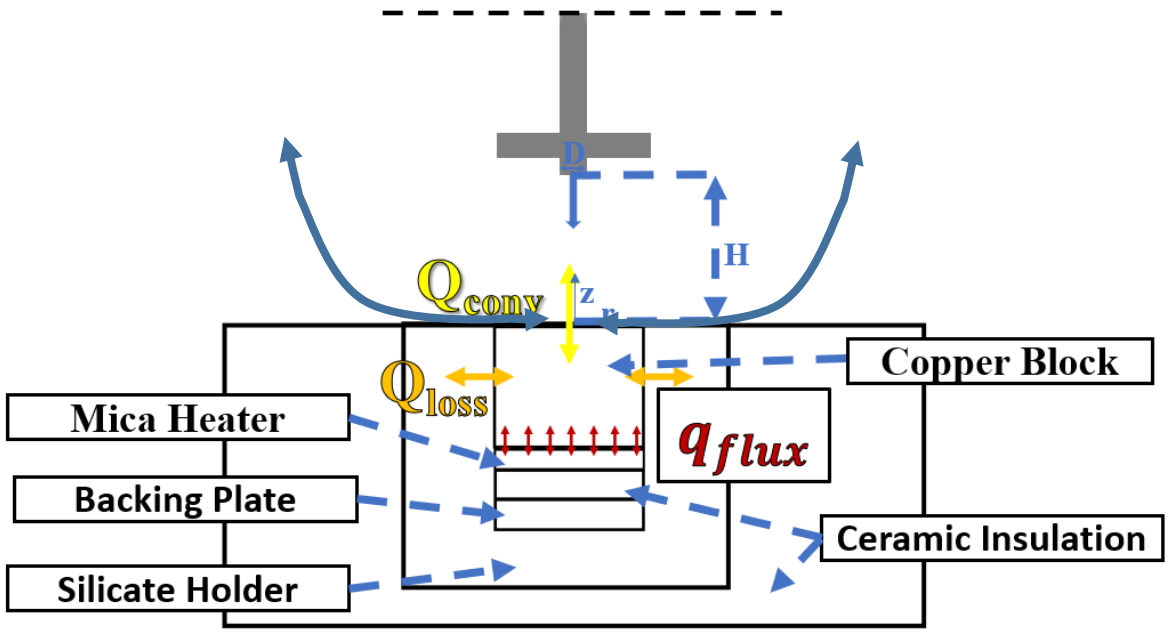

Fig. 1: Benchtop Air Setup

Rig

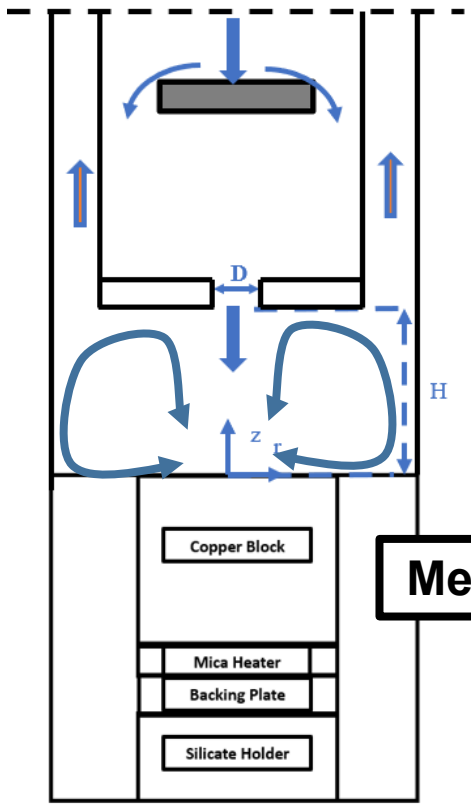

Fig. 2: Rig Confined Air Setup

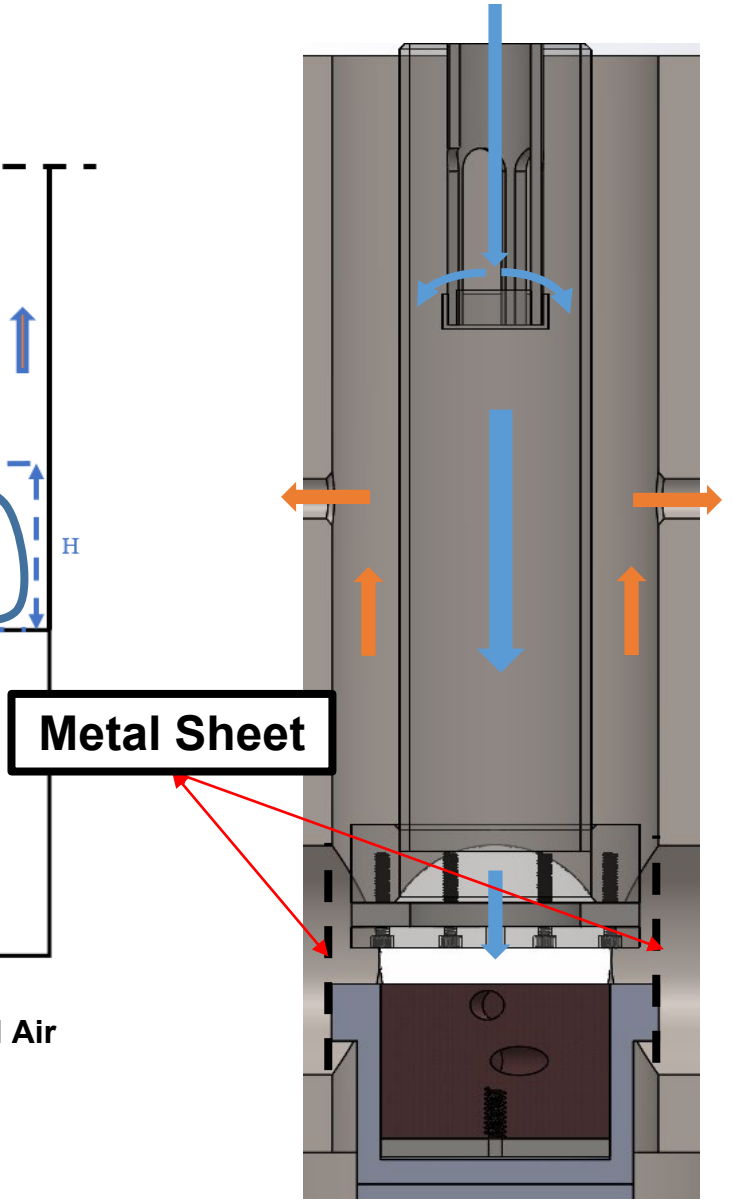

Fig. 3: Rig Confined Air Setup (model)

Rig Components

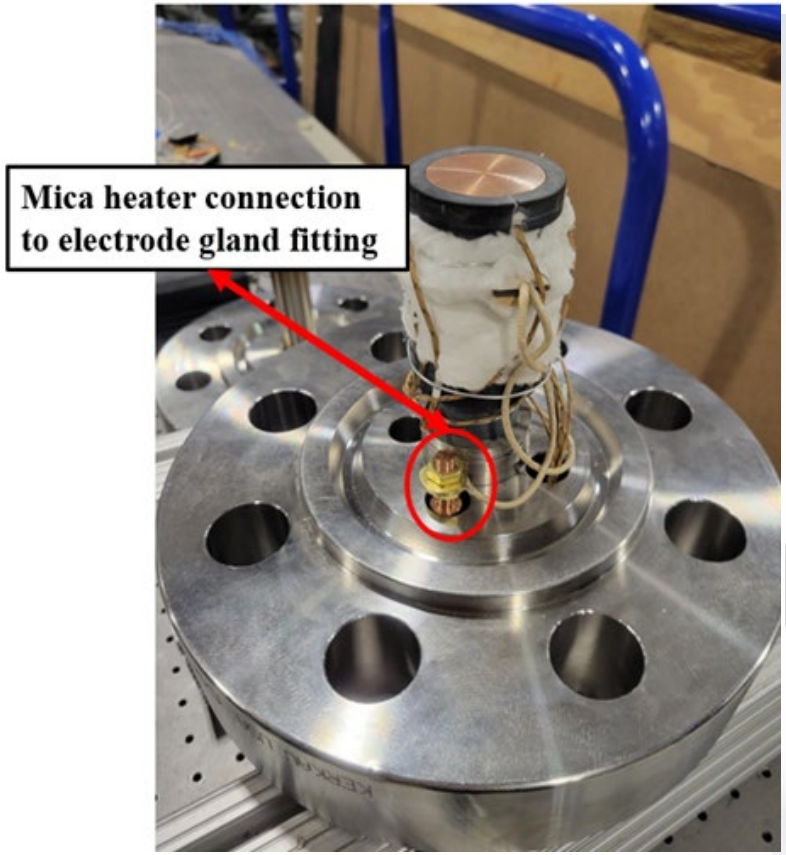

Fig. 1: Bottom Flange Assembly

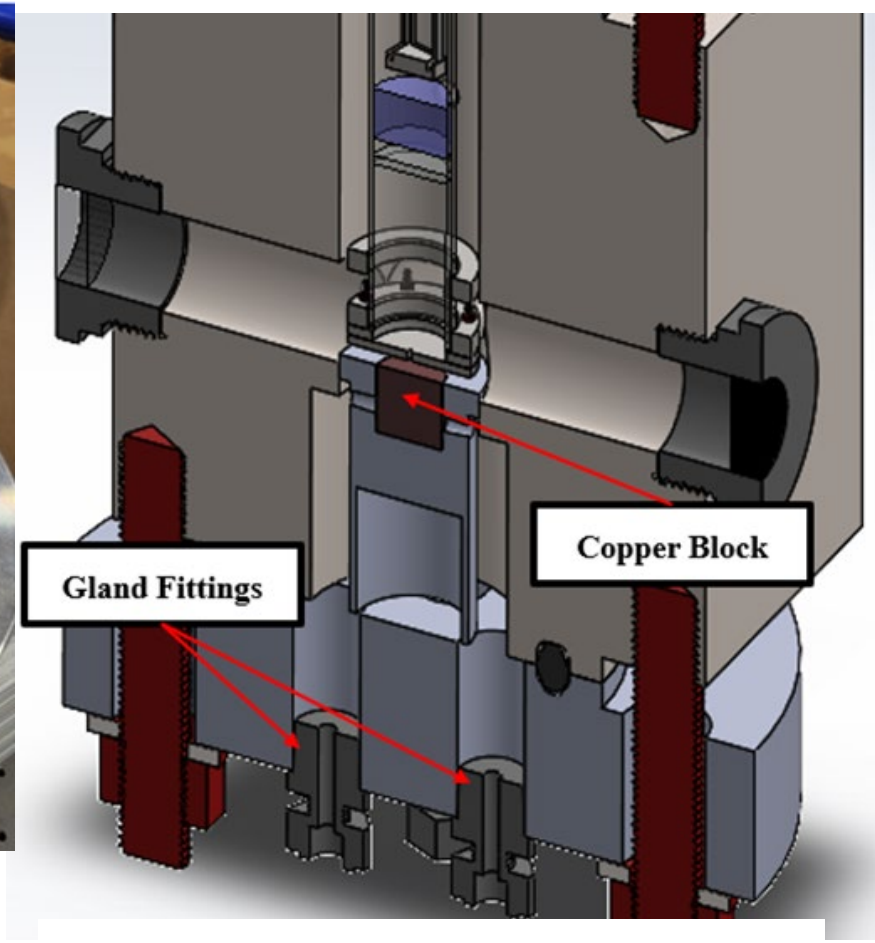

Fig. 2: Copper Block position in Pressure Vessel

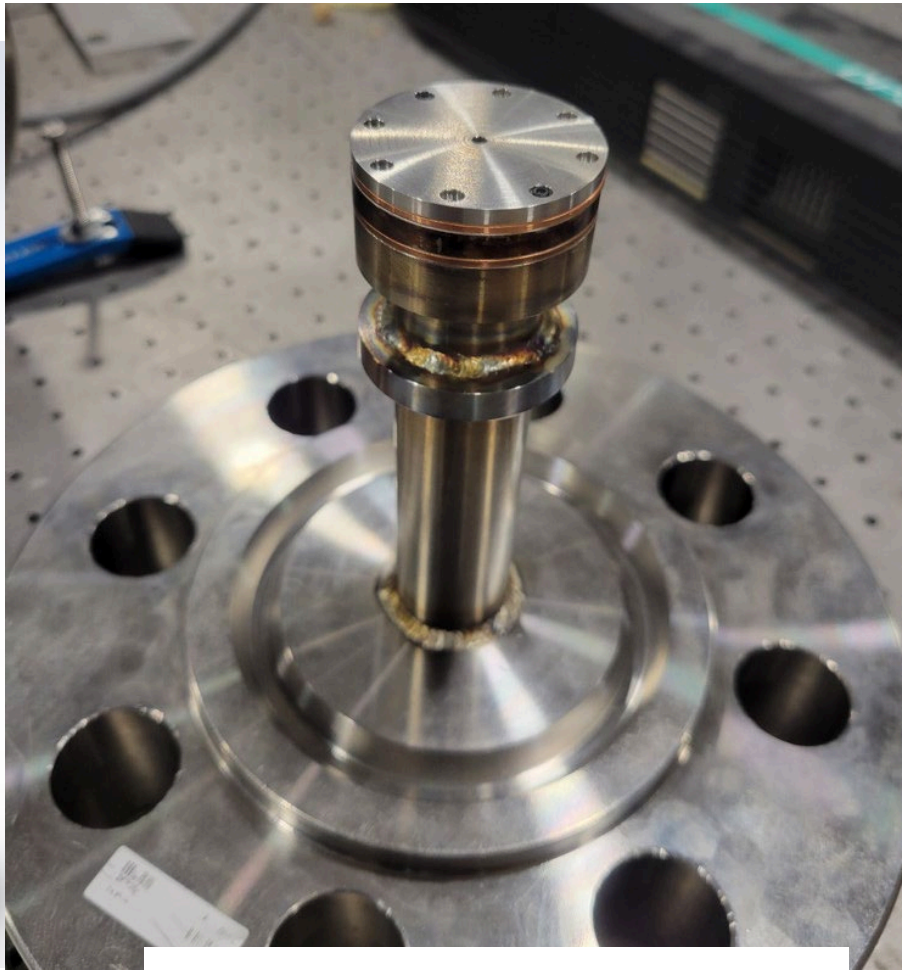

Fig. 3: Top Flange Assembly

METHODOLOGY: sCO2 Rig Setup

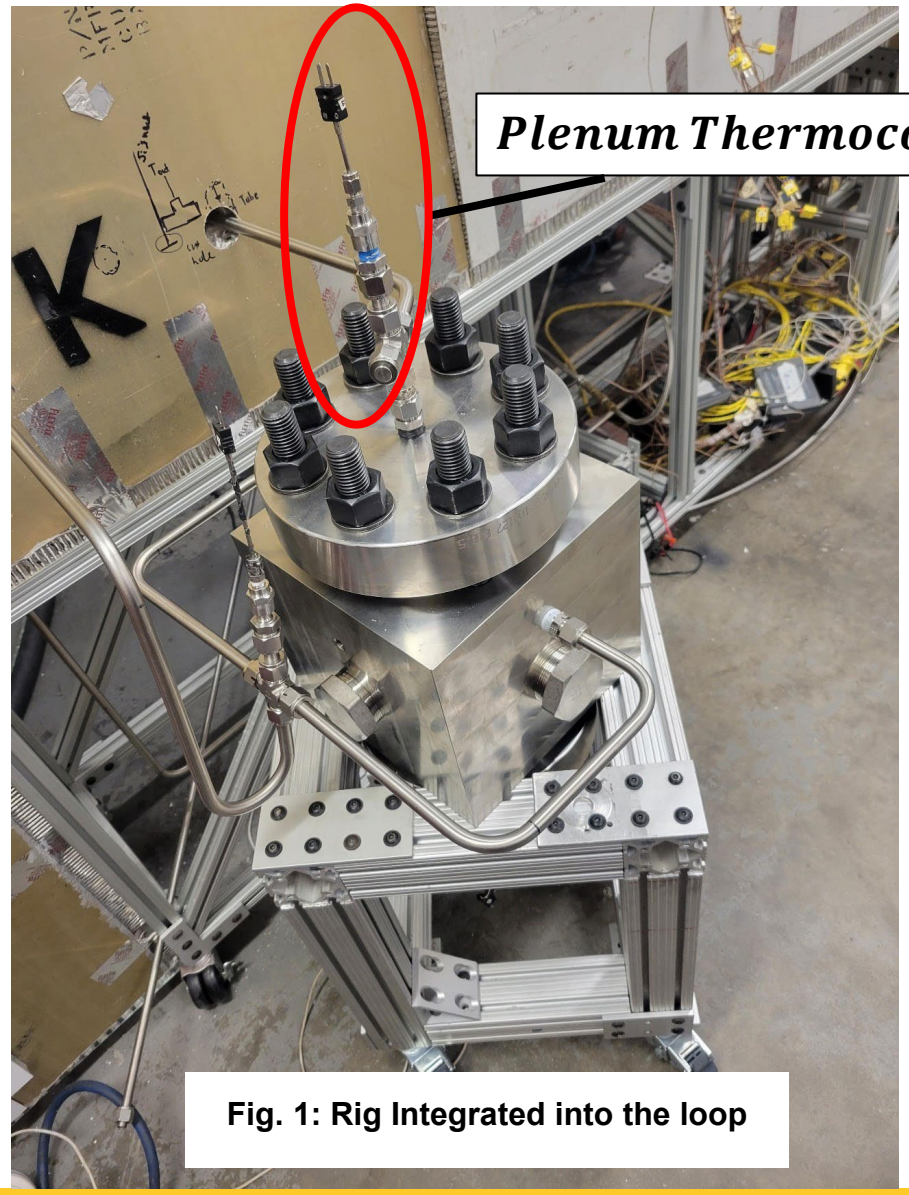

Fig. 1: Rig Integrated into the loop

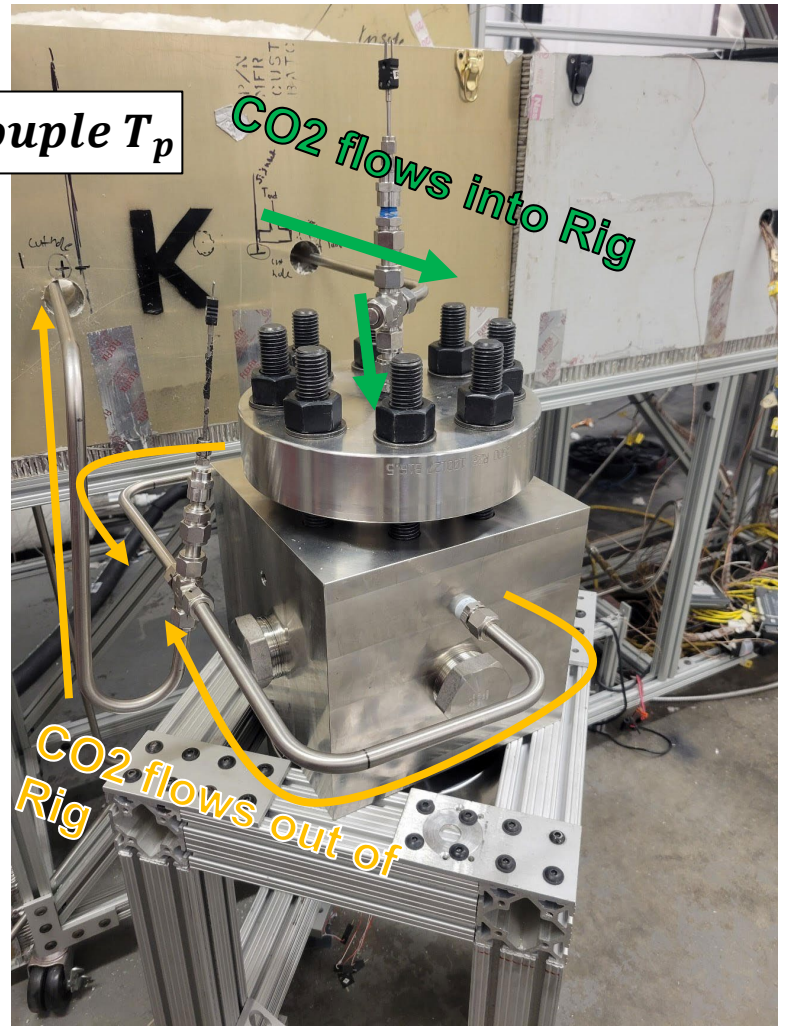

Fig. 2: CO2 flow path

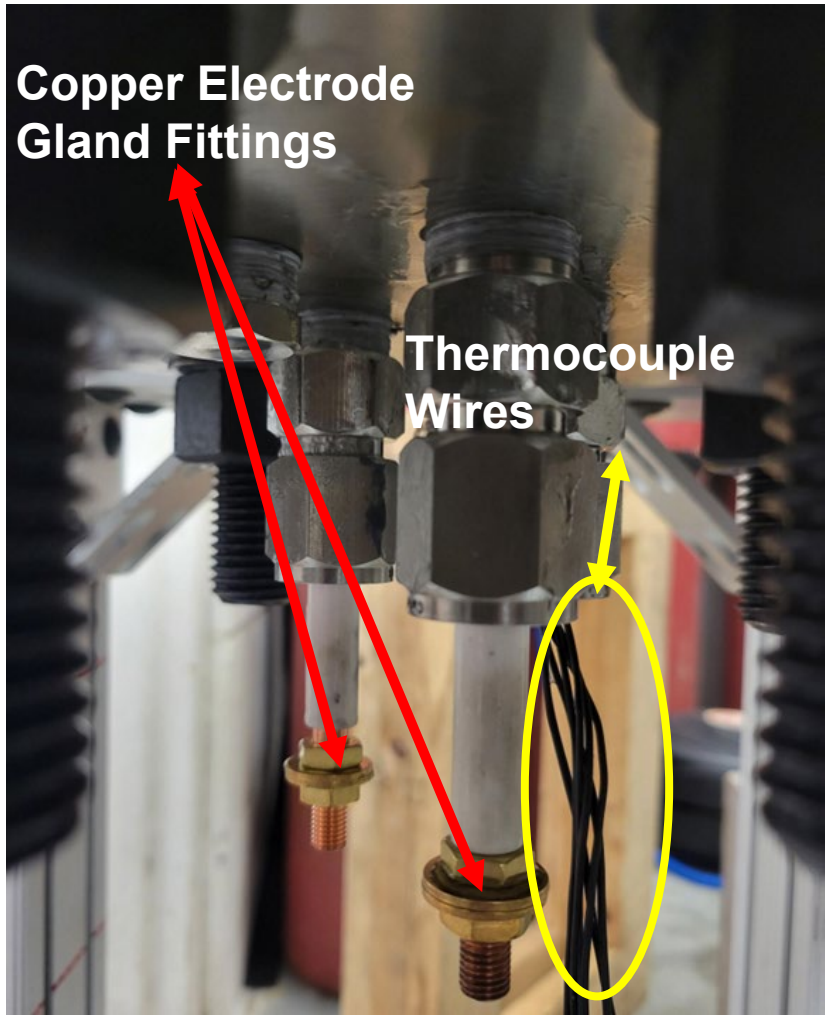

Fig. 3: Gland Fittings in bottom flange

NUMERICAL VALIDATION

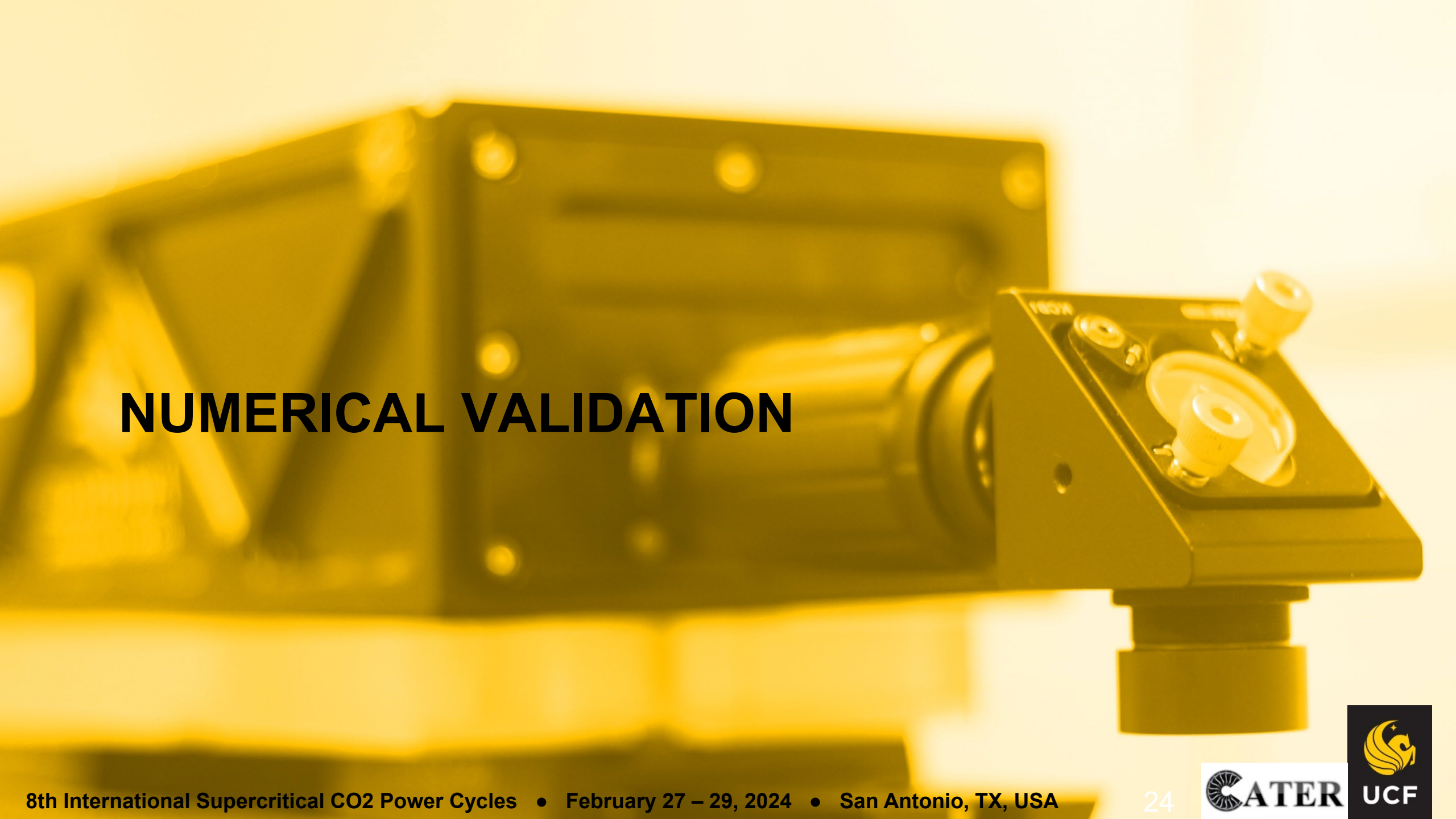

Data Reduction

- Reynolds number was calculated using the array averaged density ($\bar{\rho}$), row averaged velocity ($\bar{u}$), the diameter of the pin (D), and the array averaged dynamic viscosity ($\bar{\mu}$).

$$Re_D = \frac{\bar{\rho}\bar{u}_{max}D}{\bar{\mu}}$$

- Nusselt Number was used to understand the heat transfer of each case.

$$Nu_{avg} = \frac{\bar{h}D}{\bar{k}}$$

- The heat transfer coefficient, h, was calculated from the heat flux, Q", and the difference in temperature between the bulk fluid and the wall temperature.

$$Q" = h(T_{wall} - T_{bulk})$$

- The heat flux was derived from the energy balance using the enthalpy difference and the mass flowrate to calculate power and dividing this by the wetted area.

$$Q" = \frac{Q}{A_{wetted}} = \frac{\dot{m}}{A_{wetted}}(H_{upstream} - H_{downstream})$$

Numerical Modeling – Pin Fin

- Steady RANS turbulent models were used.
  - The Lag-EB K-epsilon turbulent model was selected to better predict the flow in the pin fin array.
- The lag elliptic blending model was introduced by Lardeau. [2016]
- This model was found to perform better than other eddy viscosity models in pin fin geometry by Otto. [2019]
  - It was observed that the LAG model better captures the vortical structures in high and low Reynolds number cases compared to other models. [2019]
- 6 cases were run using StarCCM+ with double-precision (v16.02.009-R8)
  - Three for sCO_2 and three for air to match the experimental cases.
- The initial conditions for both sets of cases can be seen in the table.
- This is a conjugate heat transfer problem, with a coupled solid and fluid domain.

Reynolds Number	Fluid	Inlet Mass Flow Rate (kg/s)	Inlet Temperature (K)	Outlet Pressure (bar)
25097	sCO_2	0.0351	679	201
49908		0.07	679	206
66598		0.0932	675	208
25171	Air	0.0215	330	31
50038		0.0427	330	31
66768		0.0571	330	31

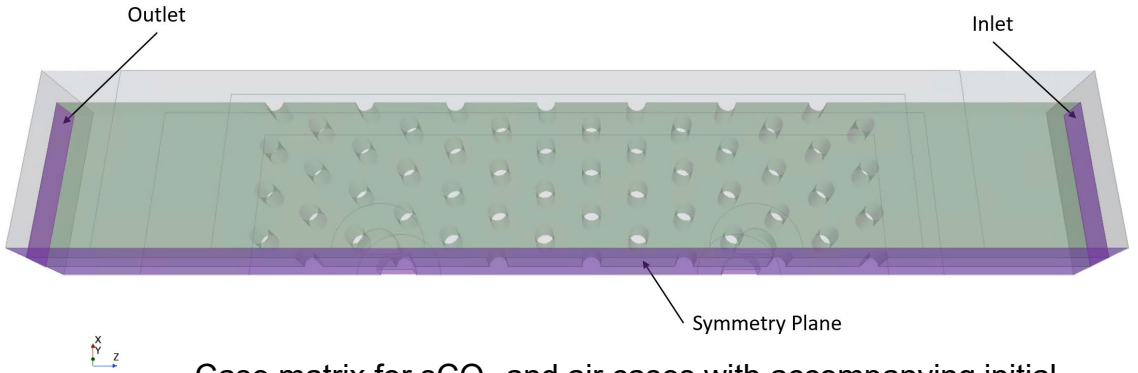

Case matrix for sCO_2 and air cases with accompanying initial flow inlet conditions and target Reynolds's number.

Numerical Modeling – Impingement

Characteristics of CFD Cases: All Simulations

- RANS-based CFD models.
- SST (Menter) K-Omega model for all cases.
- coupled flow and energy solvers used.
- All STAR-CCM+ cases performed on HPC.

Air cases:

- ideal gas
- steady state, 3D models w/ properties determined by STAR-CCM+.
- Sutherland's Law to determine dynamic viscosity & thermal conductivity.

Characteristics of CFD Cases: sCO_2 cases:

- STAR-CCM+: Coolprop used for thermophysical properties
- ANSYS Fluent: NIST tables used for thermophysical properties

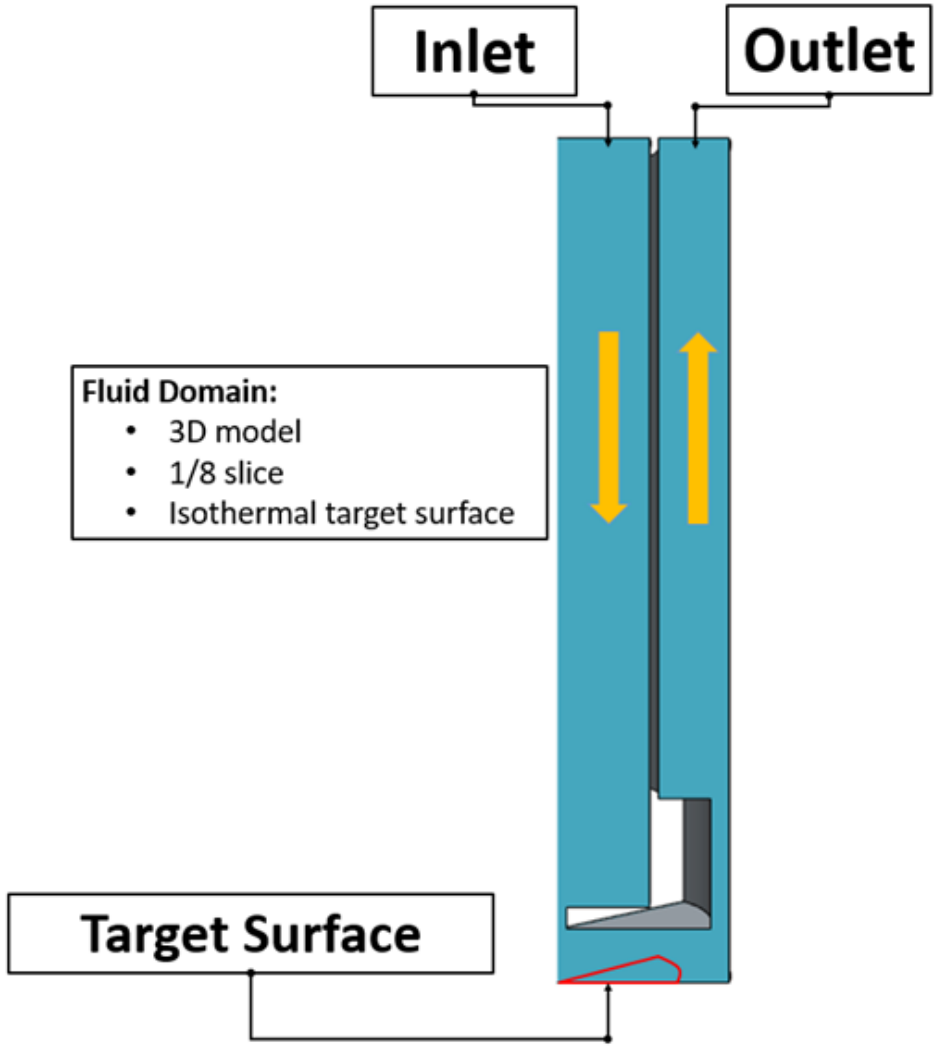

Fig 1: Fluid Domain for all simulations

RESULTS

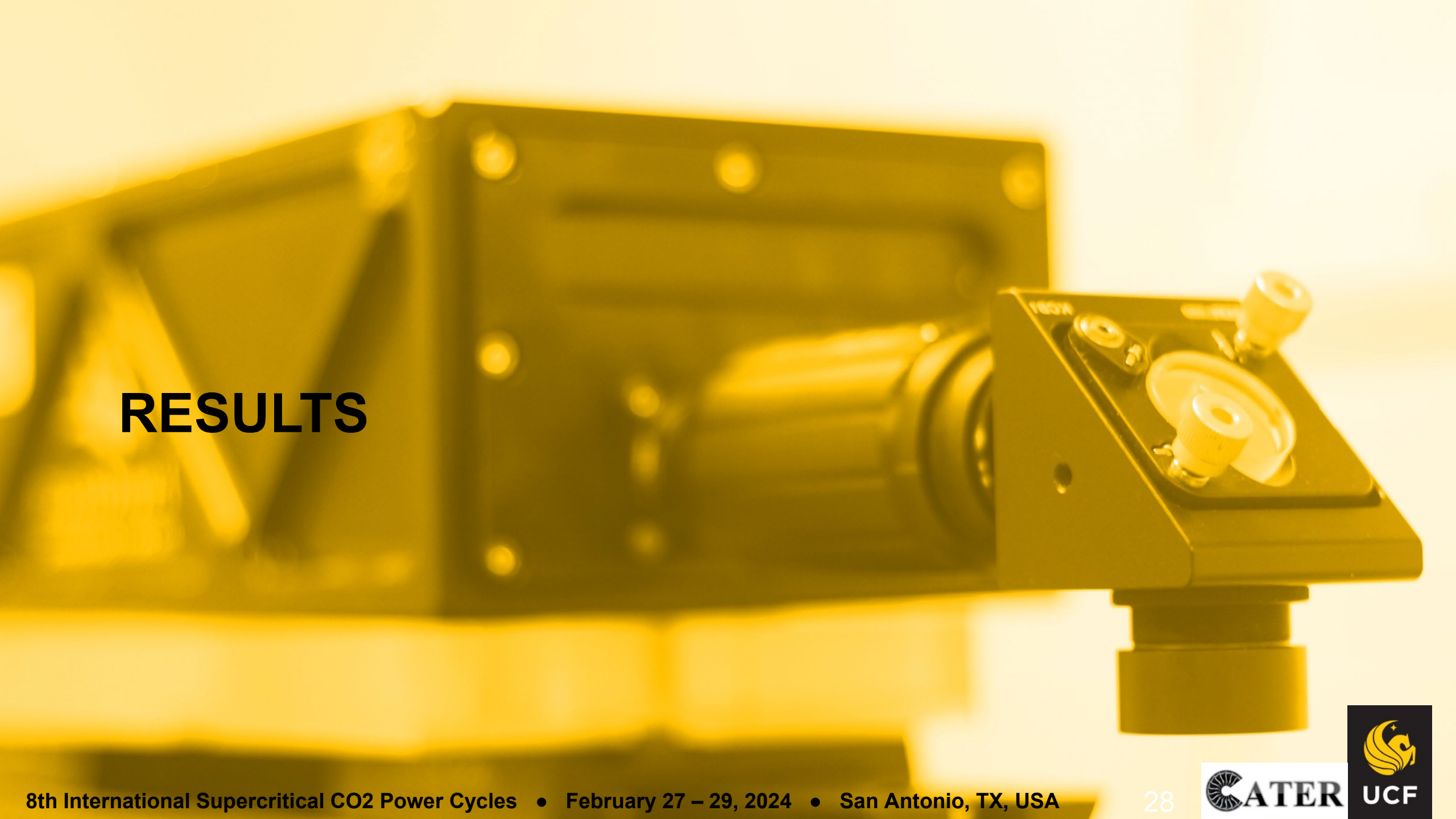

Pin Fin Experimental Heat Transfer

- The extrapolated Nusselt number for the first two cases ~25000 and ~50000 showed similar trends to Metzger correlation for air and the slightly modified correlation for sCO_2 from past CHT work. But any potential deviation is well within uncertainty.
- Above a Reynolds number of 50000, the uncertainty resulted in the overprediction of the Nusselt number.
- This required further investigation with the aid of CFD, which is why a numerical model was built from the experimentation.

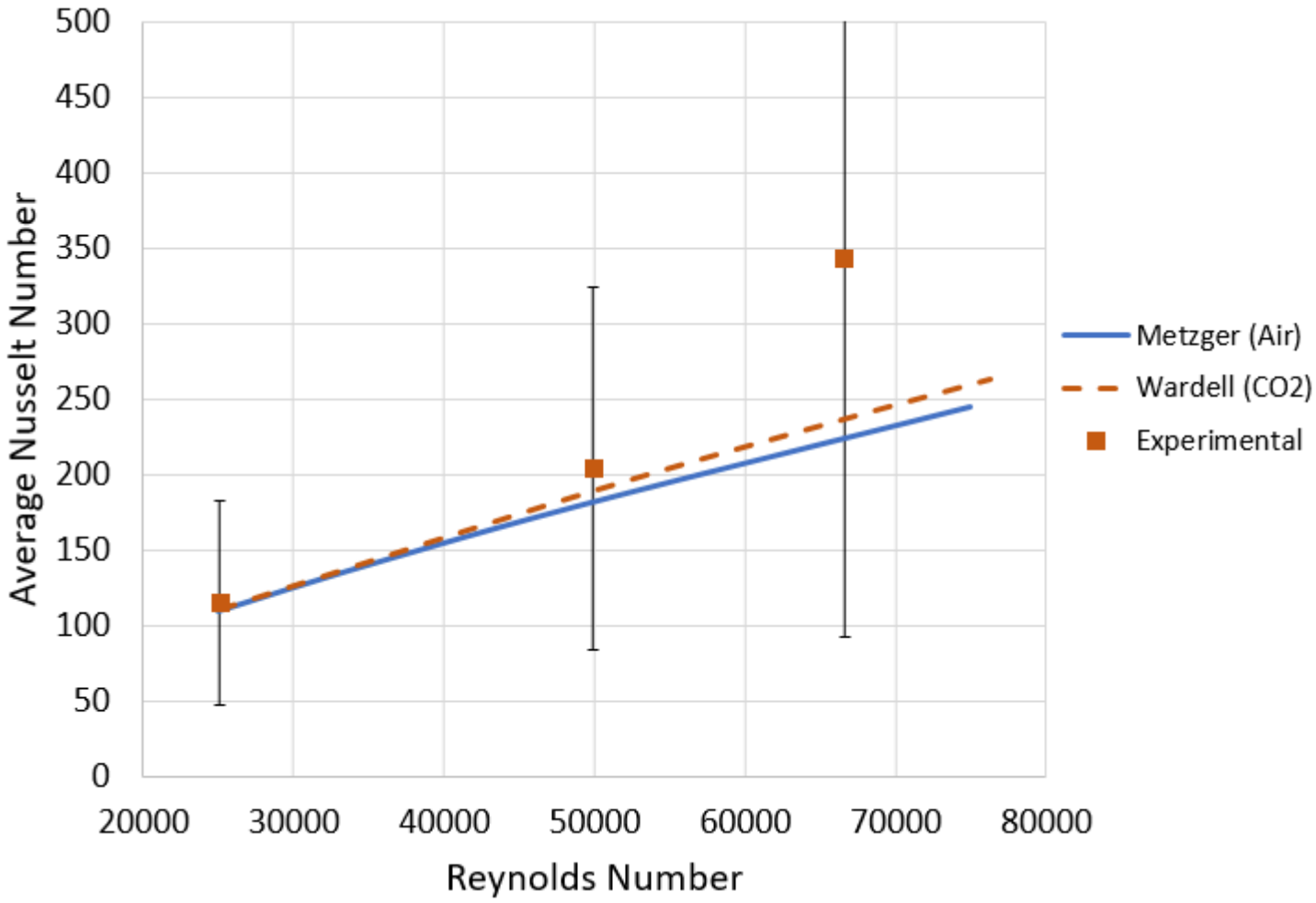

Pin Fin CFD Investigation

- Once the external heat flux was bounded to the pin fin array such as in past literary experimentation and CHT, instead of a full wall thermal boundary condition on the exterior walls, the sCO_2 showed array average Nusselt numbers larger than air cases.
  - Deviation from the slope such as in impingement is seen in CFD.
  - Experimental results were not capable of capturing local effects.
  - Experimental results only up to 50,000 Reynolds number where past CHT investigated up to 180,000

- This is where further investigation is necessary, such as local hotspots in heat transfer and creative methods of measuring local effects in high-temperature and high-pressure environments.

- It is suspected the upstream and downstream areas are having a larger impact on sCO_2 than in air.

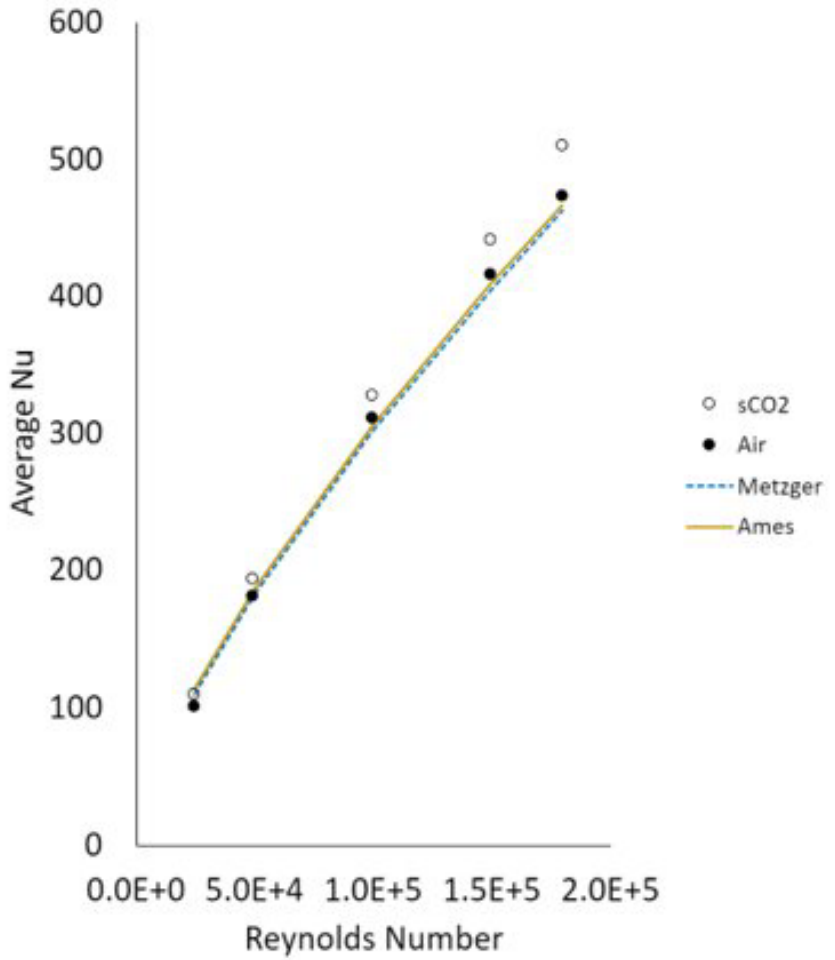

CHT results of array averaged heat transfer with local heat flux bounded to pin fin area. [Wardell 2022]

Experimental Results: sCO2 Jet Impingement

P(bar), T(°C)	Reynolds number	dT
1) 117, 154	82,932	53
2) 203, 204	256,147	15
3) 197, 225	1,157,380	3
4) 203, 320	638,993	3
5) 194, 413	105,092	9
6) 95, 412	197,393	11
7) 209, 416	249,984	8
8) 197, 415	401,103	5
9) 179, 413	470,112	5
10) 191, 405	583,443	4
11) 202, 400	601,530	4

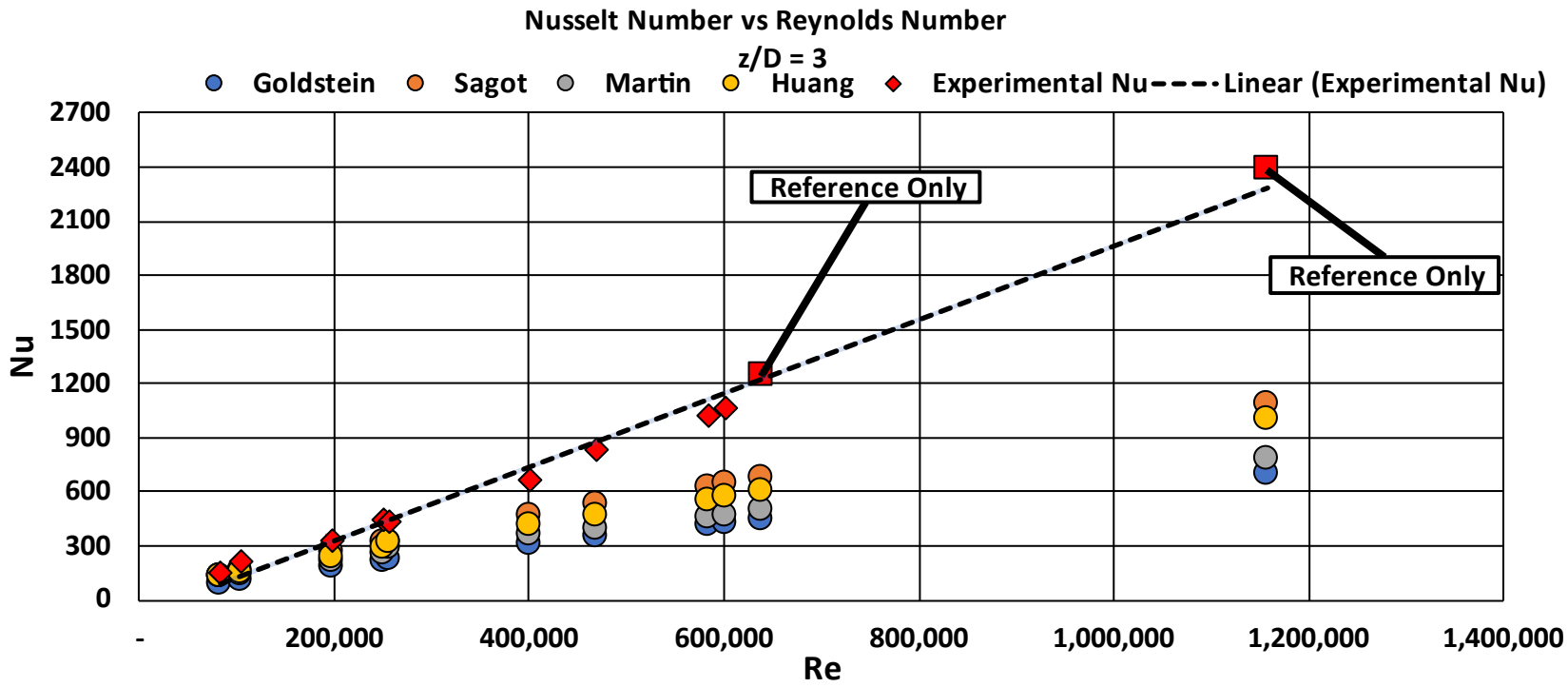

Fig. 1: Complete sCO2 experimental data set: Reference Only points are shown to evaluate the impact on the trendline

- Test 5-11 used to develop correlation
- Lines average deviation from target data set ≈ 12%

CFD Results: sCO2 Jet Impingement

sCO2 Cases:

- Primary conditions for experiments: 200 bar 400 °C
- (2) STAR-CCM+ & (3) Fluent
- The CFD cases corroborate discrepancy between experimental results & air derived correlations
- **Air-correlations don't match sCO2 values.**

CFD	Re #	Exper. Nu	CFD Nu	% deviation
STAR-CCM+	100,508	221	186	16%
ANSYS-Fluent	197,768	335	335	—
STAR-CCM+	249,985	446	394	12%
ANSYS-Fluent	470,112	836	757	9%
ANSYS-Fluent	601,616	1,071	989	8%

Table 1: CFD % deviation from experimental results

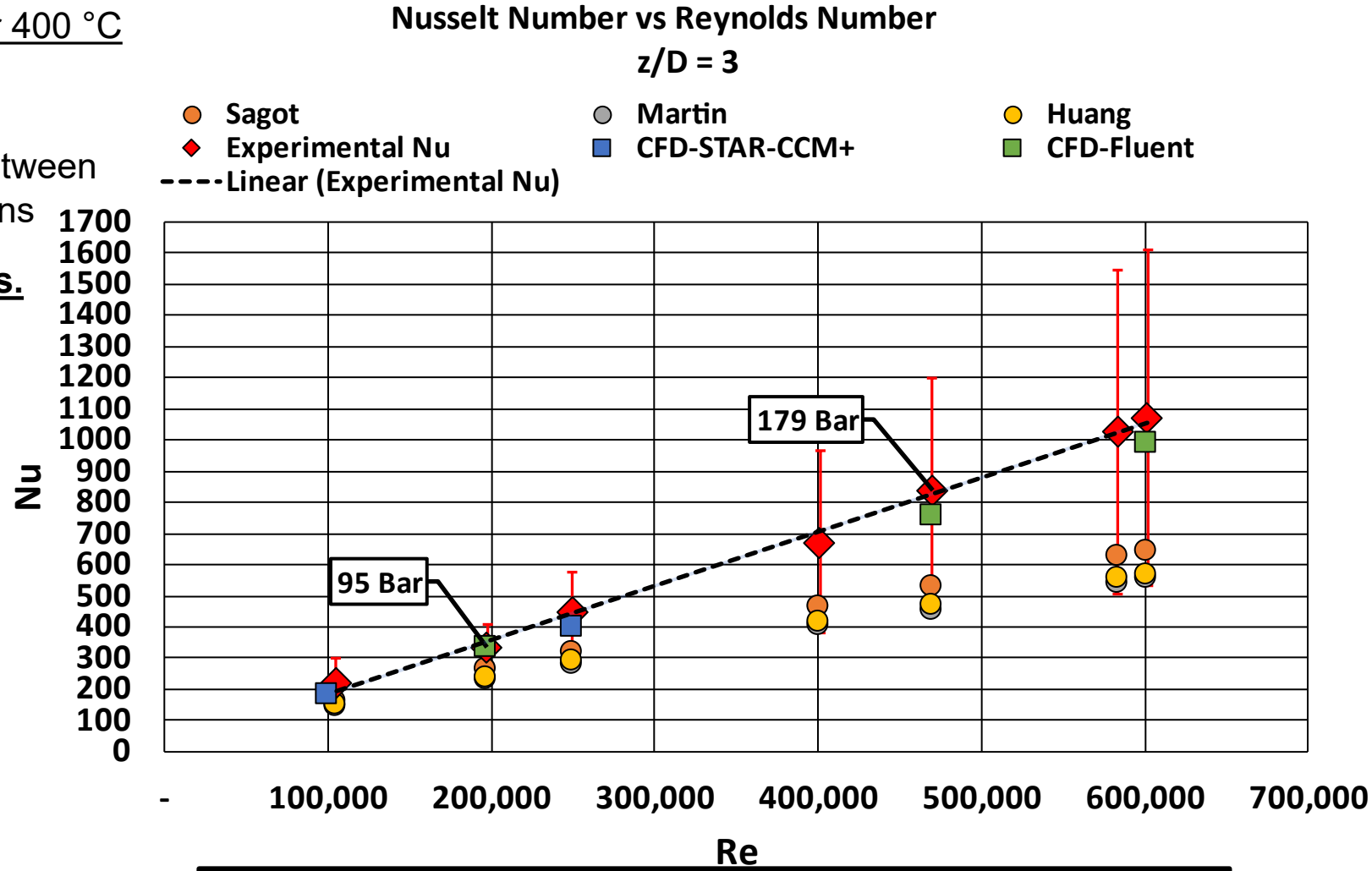

Fig. 1: sCO_2 Rig Test Results z/D= 3 at primary conditions

Results: sCO2 Jet Impingement

Table 1: Adjusted Martin deviation from experimental data

Reynolds Number	Deviation from sCO_2
105,092	3%
197,393	12%
249,984	3%
401,103	7%
470,112	1%
583,443	6%
601,530	9%

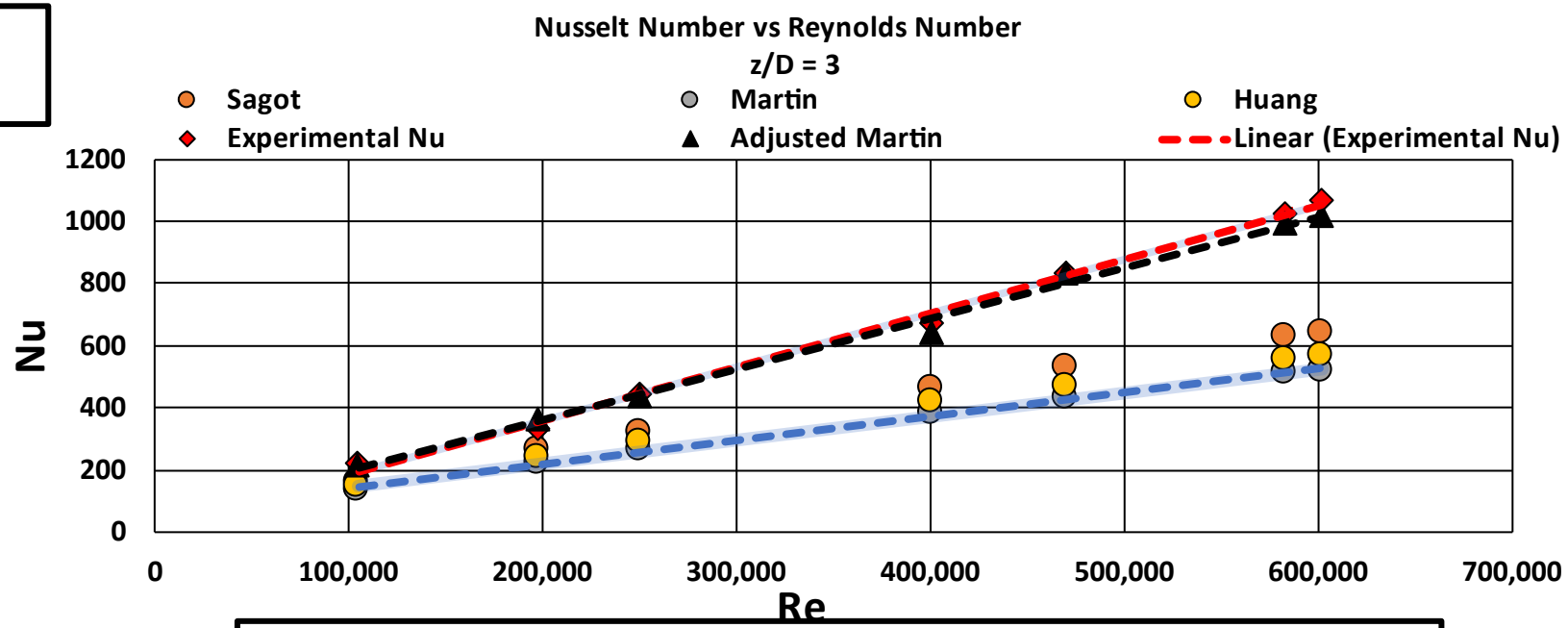

Fig. 1: Adjusted Martin plotted w/ experimental data

Adjusted Martin Correlation:

$$Nu_{avg} = Pr^{0.42}\frac{D}{r}\frac{1-1.1D/r}{1+0.1\left(\frac{H}{D}-6\right)D/r}0.151Re^{n},$$

$$for\ 100{,}000 < Re < 360{,}000,\ \mathrm{n} = 0.8158$$
$$for\ 360{,}000 < Re < 601{,}000,\ \mathrm{n} = 0.8253$$

$$\text{When } T_j \approx 400\ ^{\circ}\mathrm{C}\ , 95 < \mathrm{P(bar)} < 210, \frac{\mathrm{H}}{\mathrm{D}} \approx 2.8$$

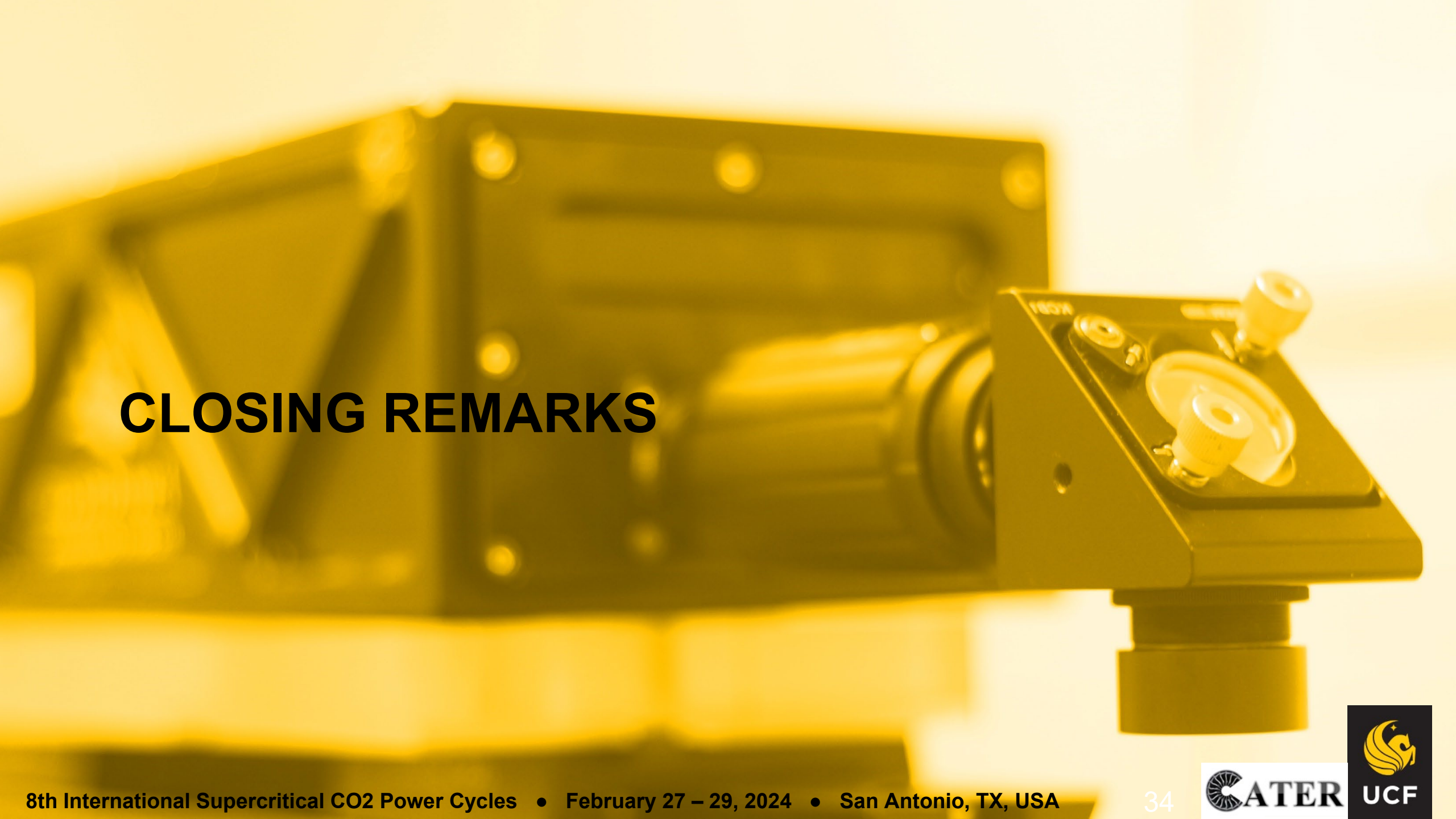

CLOSING REMARKS

Summary of Main Results

- SCO_2 jet impingement provides more heat transfer than predicted by air-derived correlations, making air correlations unable to capture the heat transfer of jet impingement in the sCO2 environment. This led to an adjusted Martin correlation to be derived to represent the new trend of jet impingement in the sCO2 environment.
- Both STAR-CCM+, and ANSYS Fluent showed excellent performance with <15 % deviation in predicting sCO2 heat transfer in the evaluated Reynolds Number range for internal cooling geometry from experiments.
- At the lower Reynolds numbers for pin fin, less than 50000, strong correlations to existing data from Ames [Ames 2005] and Metzger [Metzger 1982] and CFD analysis done in previous investigations are presented. However, this seemed to possibly under-predict the heat transfer when compared to CFD simulations for a full exterior heat flux boundary like in this experiment.
    - Under 50000 Reynolds number, correlations derived by air data were able to represent the heat transfer of the sCO2 pin fin array within experimental uncertainty.

Acknowledgments

- This material is based upon work supported by the Department of Energy, United States of America under award number DE-FE0031929. This paper was prepared as a part of work sponsored by an agency of the United States Government in partnership with Southwest Research Institute, General Electric Global Research Center, 8Rivers Capital LLC, Air Liquide, the Electric Power Research Institute, University of Central Florida, and Purdue University.
- M. Otto would like to further acknowledge the support from the University of Central Florida's Preeminent Postdoctoral Program (P3).
- Lastly, the authors acknowledge the University of Central Florida Advanced Research Computing Center for providing computational resources and support that have contributed to results reported herein. URL: https://arcc.ist.ucf.edu

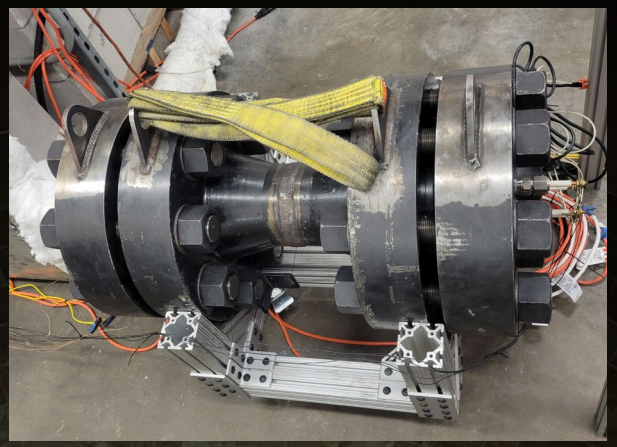

Thank you for your attention

Emmanuel Gabriel-Ohanu

Emmanuel.Gabriel-Ohanu@ucf.edu

University of Central Florida

Center for Advanced Turbomachinery and Energy Research

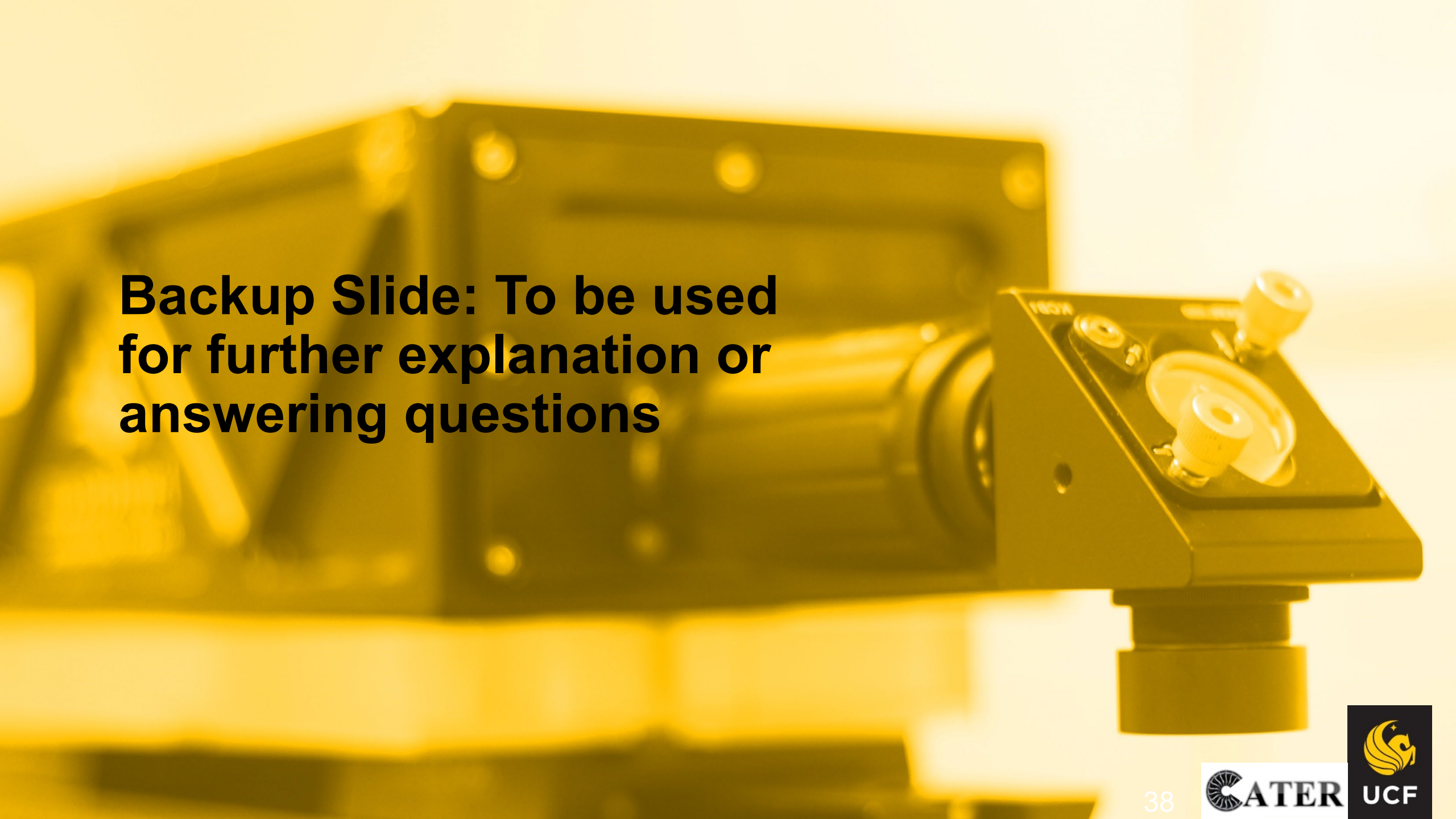

Backup Slide: To be used for further explanation or answering questions

Full Internal Assembly

- A filter equalized the pressure vessel to the same pressure as the test section while ensuring insulation didn't enter the loop.
- Achieved a near zero pressure difference across test section walls.
- UNITHERM Aluminum Silicate Fiber Blanket Insulation was used to wrap the test section and fill the pressure vessel cavity

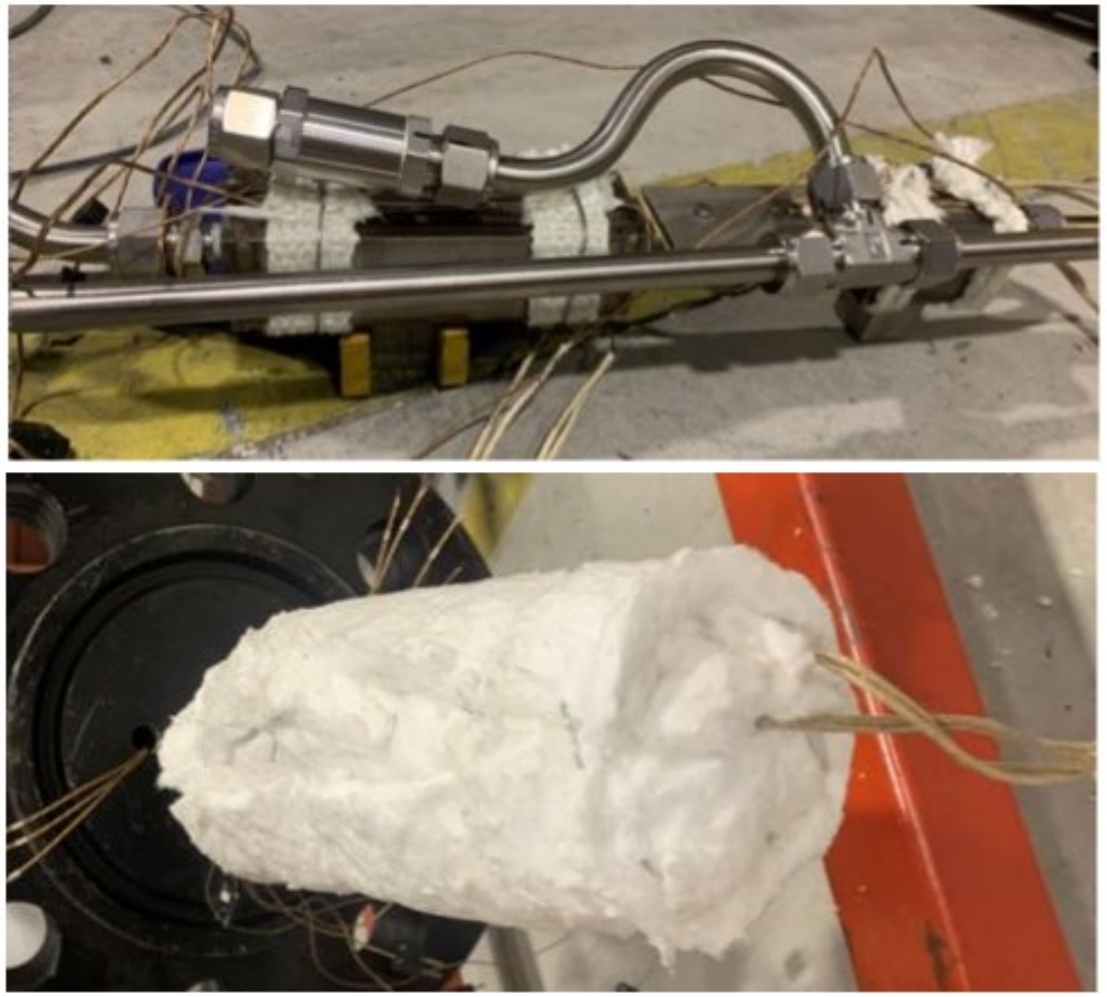

Plumbed and wrapped internal assembly

Instrumentation

- Conax gland fittings on the outside allowed seven J-type thermocouples to pass into the vessel. Four Conax gland fittings for copper electrodes were used to pass voltage to two Minco mica heaters inside the rig.

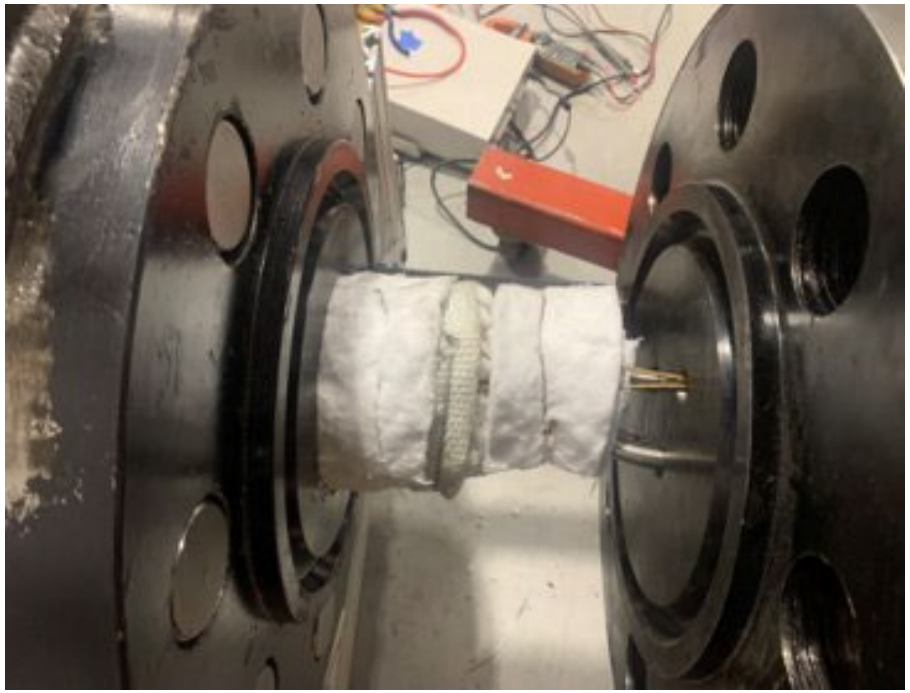

Wrapped assembly with thermocouple wires

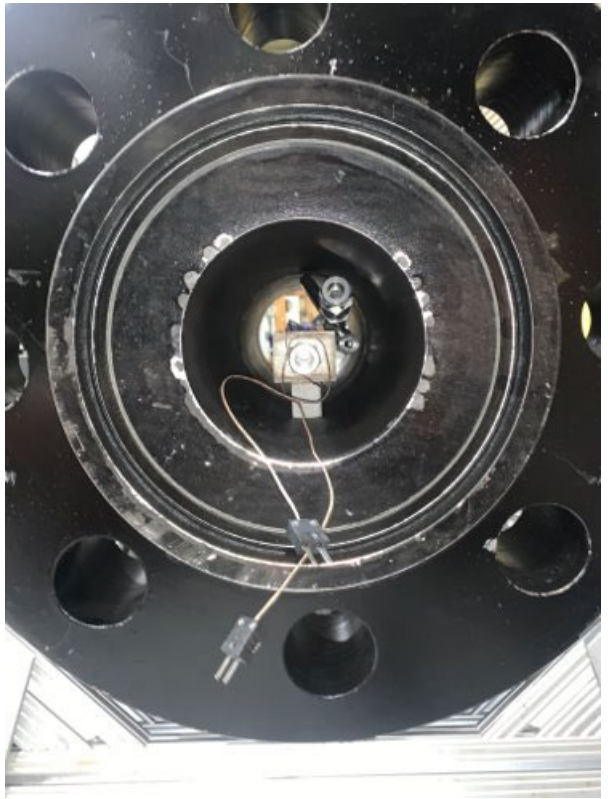

Internal Assembly sitting inside pressure vessel

METHODOLOGY: Bottom Flange Assembly

Fig. 1: Copper electrode gland fitting

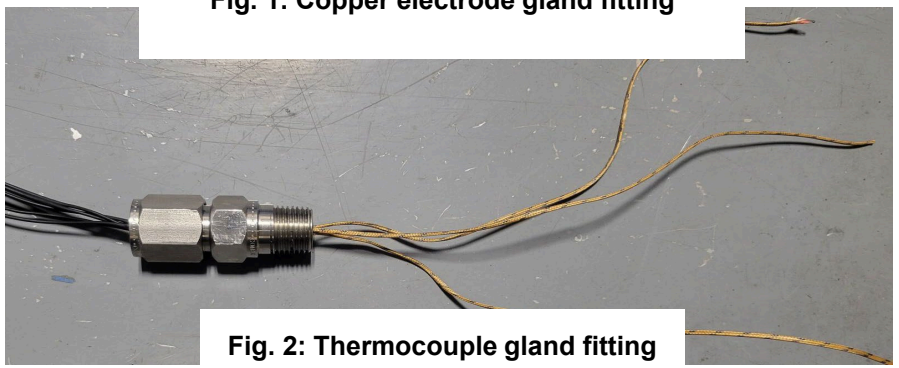

Fig. 2: Thermocouple gland fitting

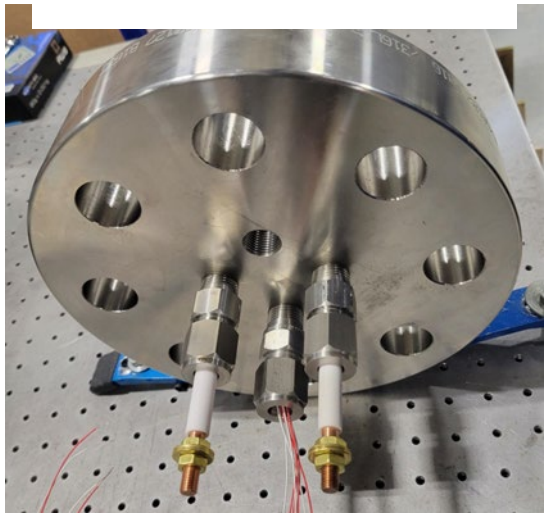

Fig. 3: Gland fitting instrumentation

Mica heater connection to electrode

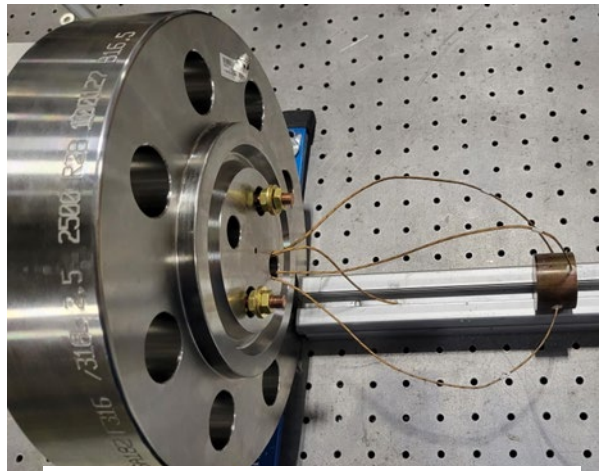

Fig. 4: Copper block instrumentation

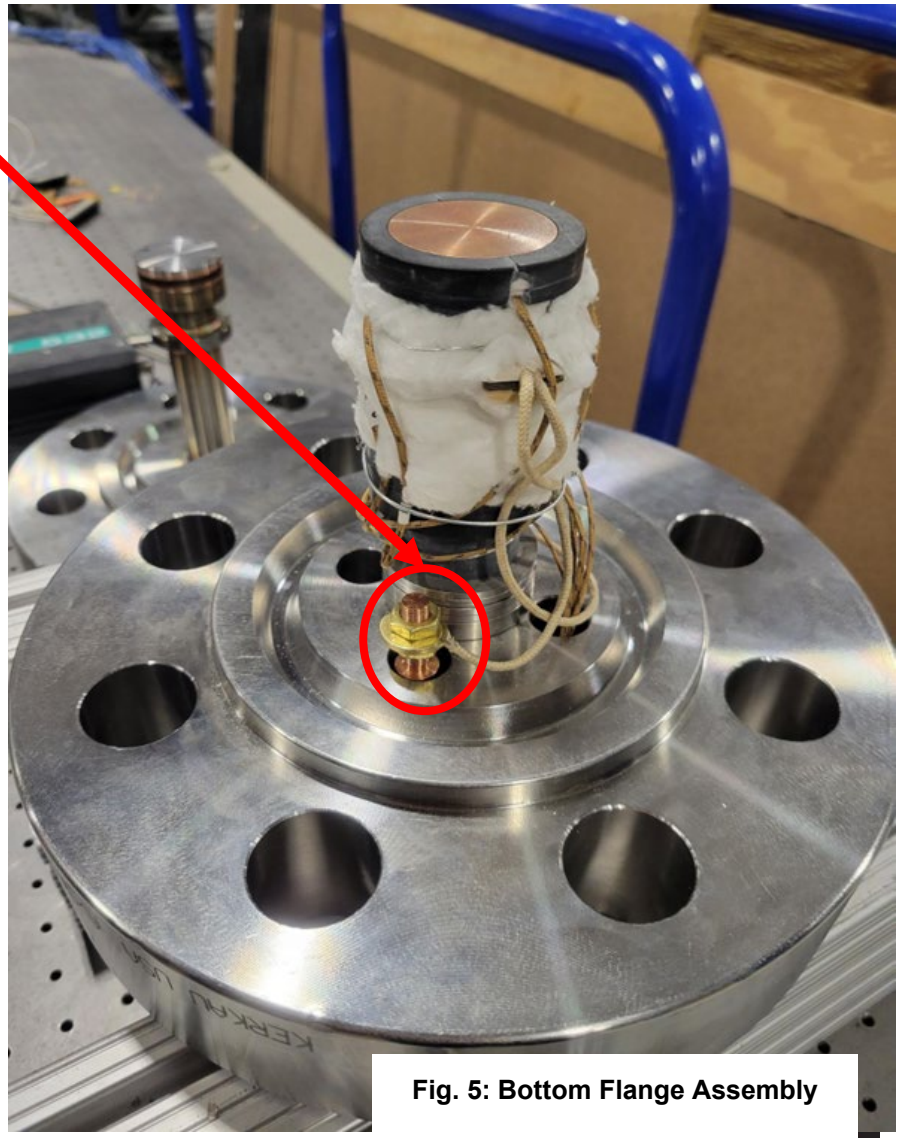

Fig. 5: Bottom Flange Assembly

METHODOLOGY: Top Flange Assembly

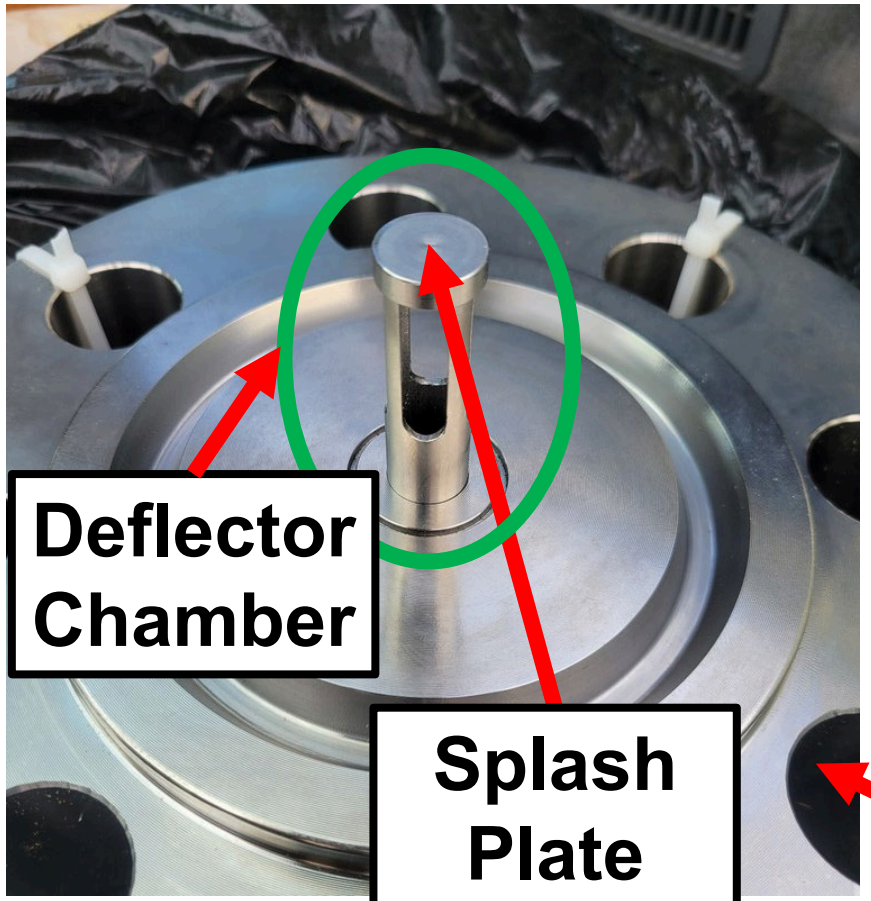

Fig. 1: Deflector Chamber

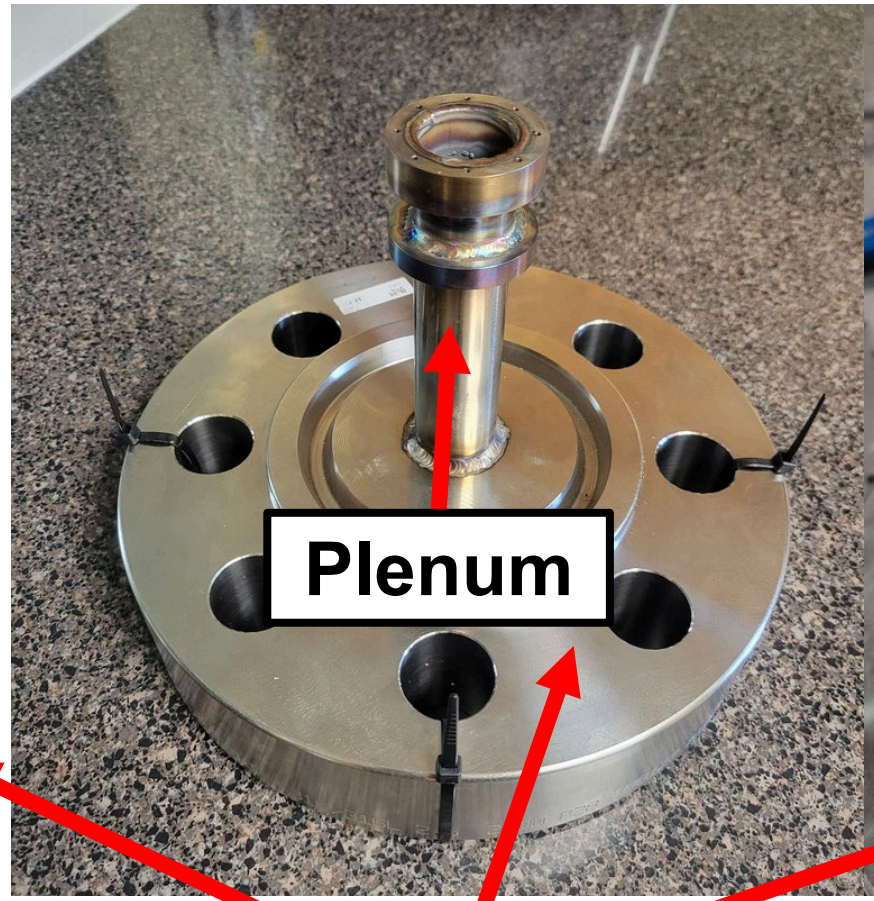

Fig. 2: Plenum

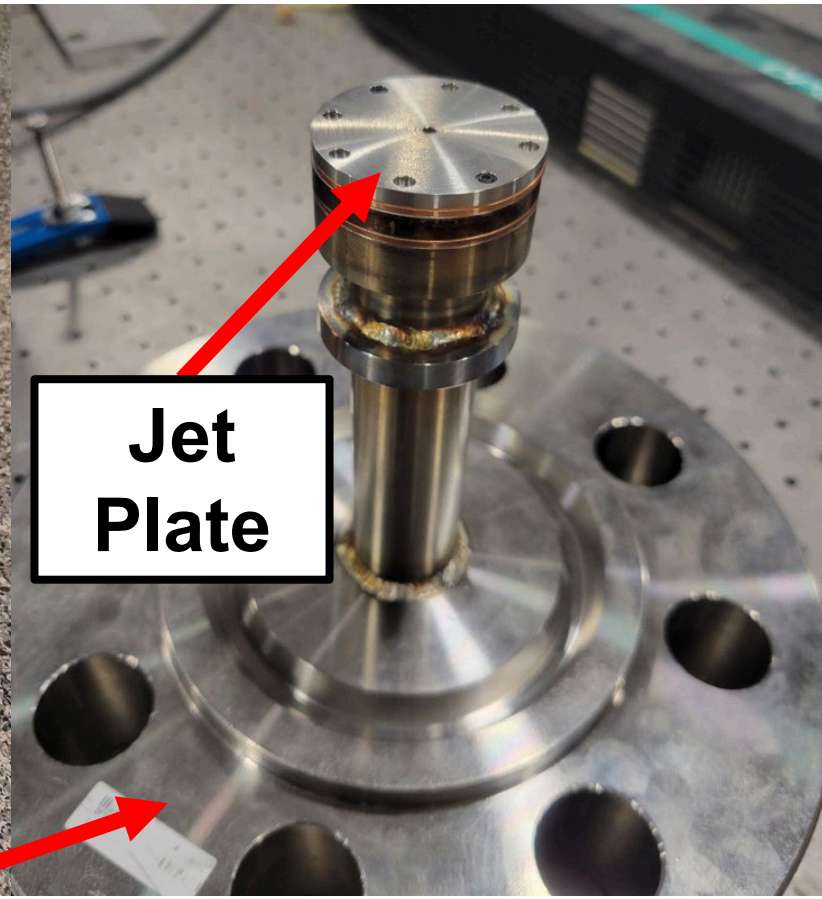

Fig. 3: Jet Plate

Top Flange

Surface Temperature

- **Goal:**
  - Extrapolate surface temperature values for benchtop & rig tests
- **Required Conditions**
  - Steady state conditions
  - constant heat flux, no heat generated
  - constant thermal conductivity
- **<u>Conditions apply to all test.</u>**
- Slope and intercept will change based on temperatures for each test

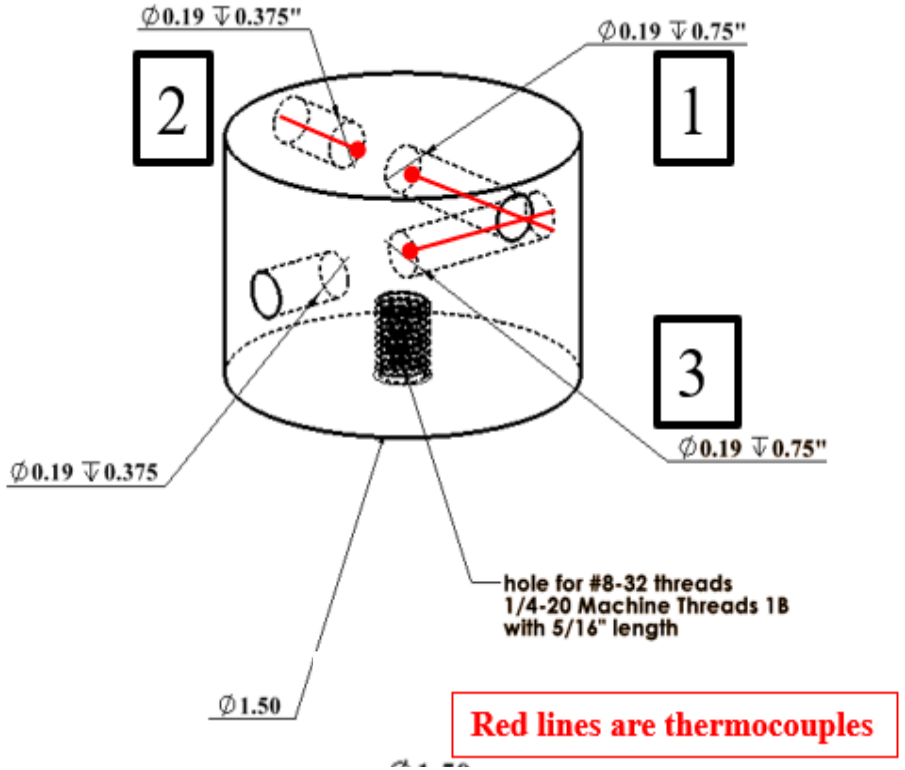

Fig. 1: Copper Block w/ thermocouple holes ISO view

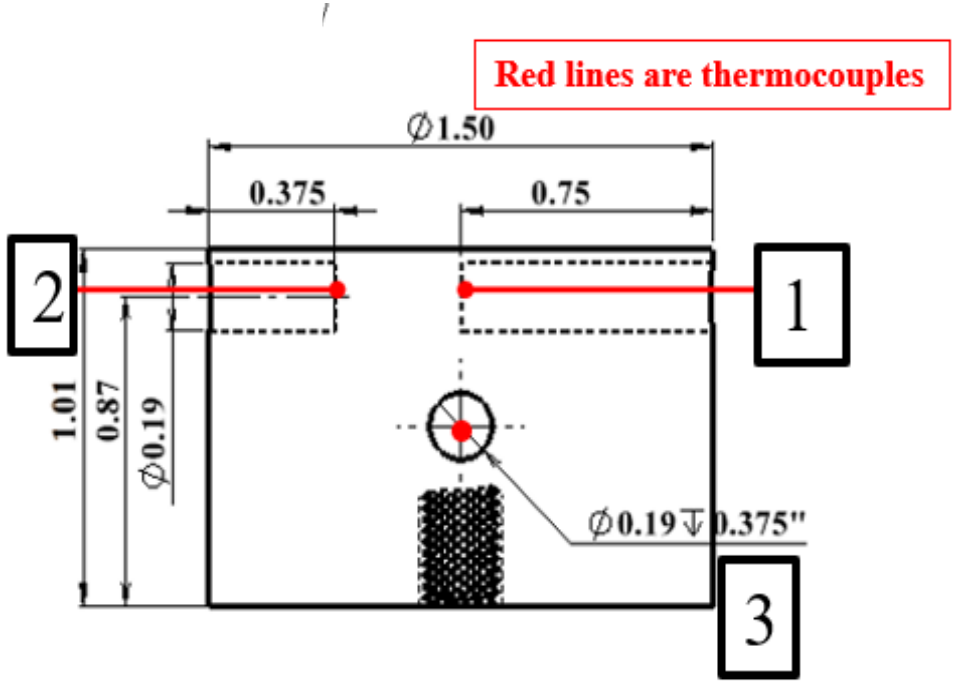

Fig. 2: Copper Block w/ thermocouple holes cross-sectional view

METHODOLOGY: Surface Temperature

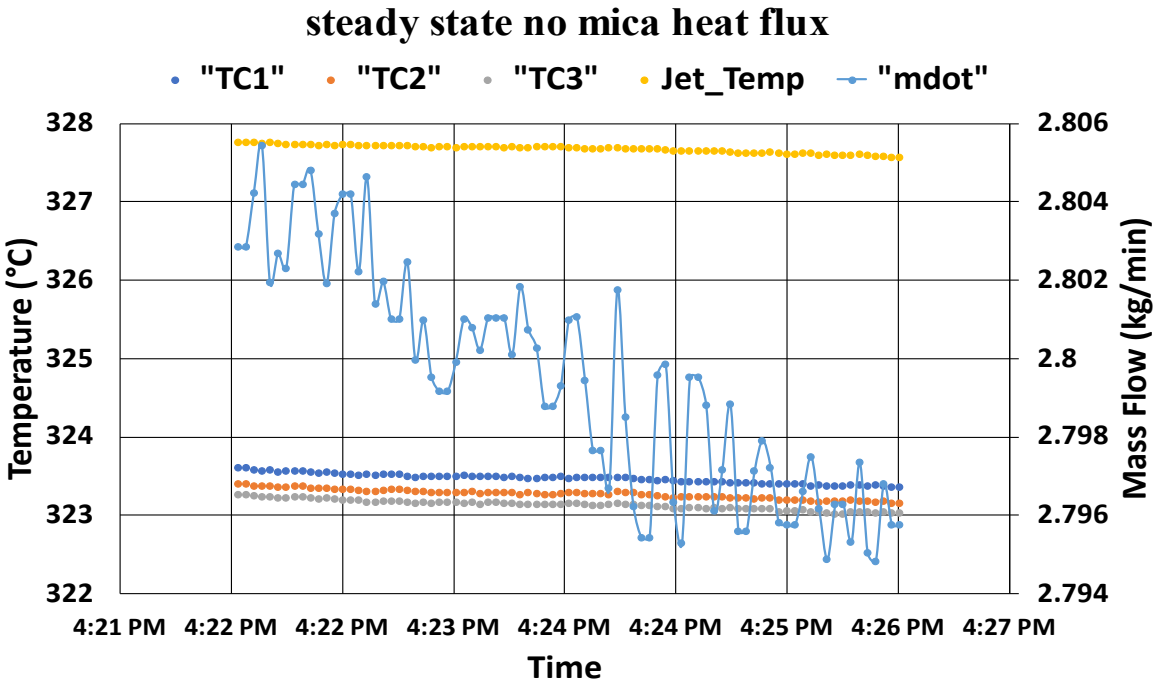

Fig. 1: Steady Temperature & Mass Flow Conditions

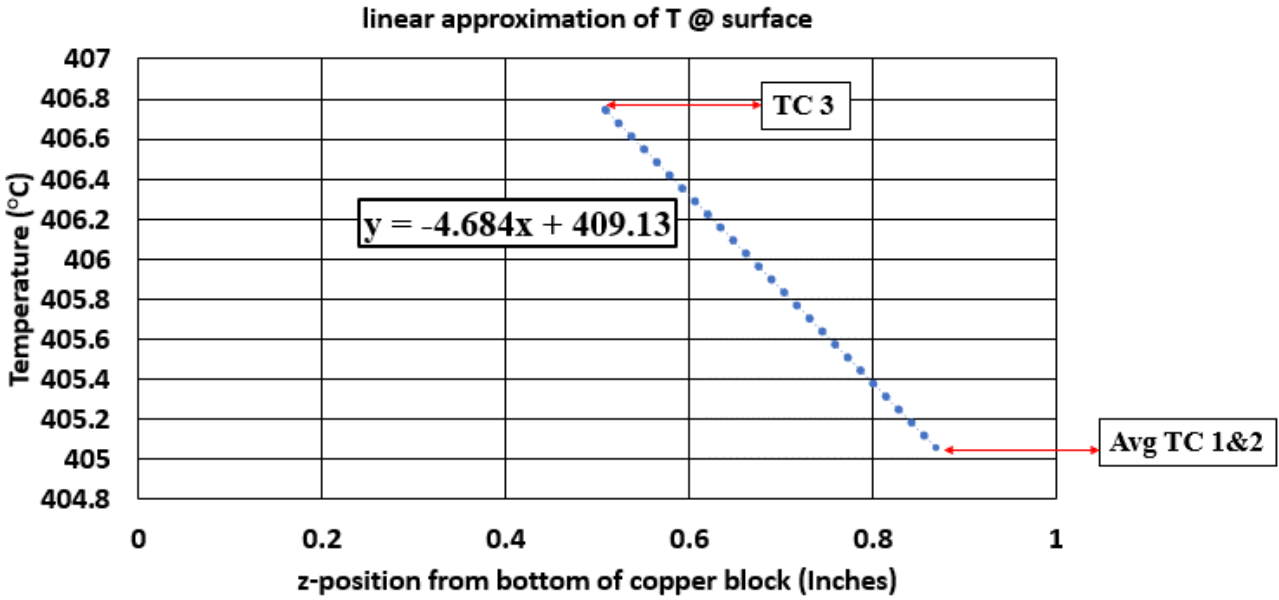

Fig. 2: z-position is the location normal the copper block surface.

Y= 404.4 degree C @ Copper block Surface i.e., X=1

METHODOLOGY: Heat Loss Test

Goal:

- *Approximate heat loss when convection is present.*

- Experimental setup has a 2 in rohacell block over the copper block
- Rohacell thermal conductivity is approximately = 0.02 W/m*C
- A ceramic fiber insulation w/ thermal conductivity = 0.029 W/m*C surrounds the copper block
- Delta T is the temperature difference between the rig surface and the copper block
- Qsupply is measure wattage supplied from mica heater

$$\text{Equ 1: } q_{flux} \times A = Q_{supply} = Q_{convection} + Q_{loss} \text{ (W)}$$

$$\text{Equ 2: } Q_{supply} = \frac{V^2}{R} = Q_{loss} \text{ (W)}$$

- Where V is voltage across the mica heater
- And R is the mica heater resistance
- This was done to quantify the conduction losses within the system

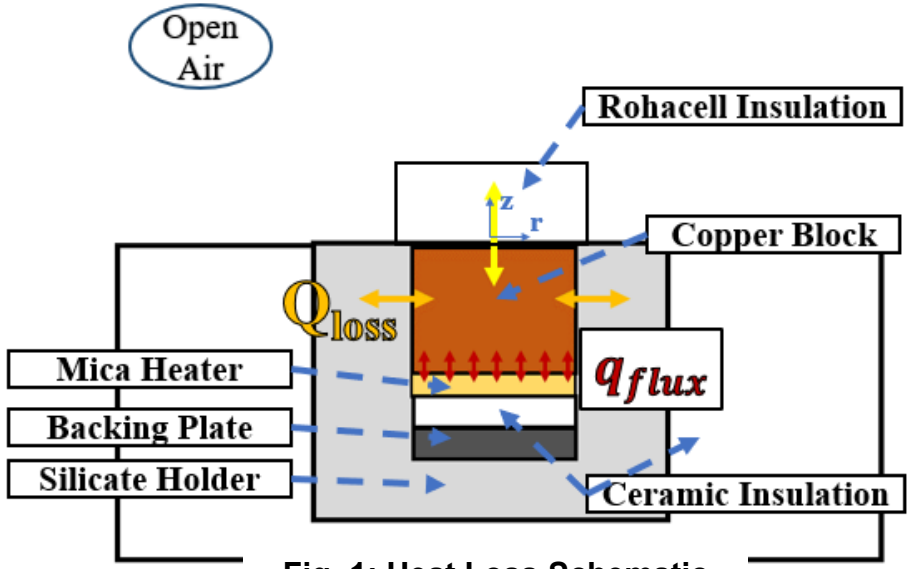

Fig. 1: Heat Loss Schematic

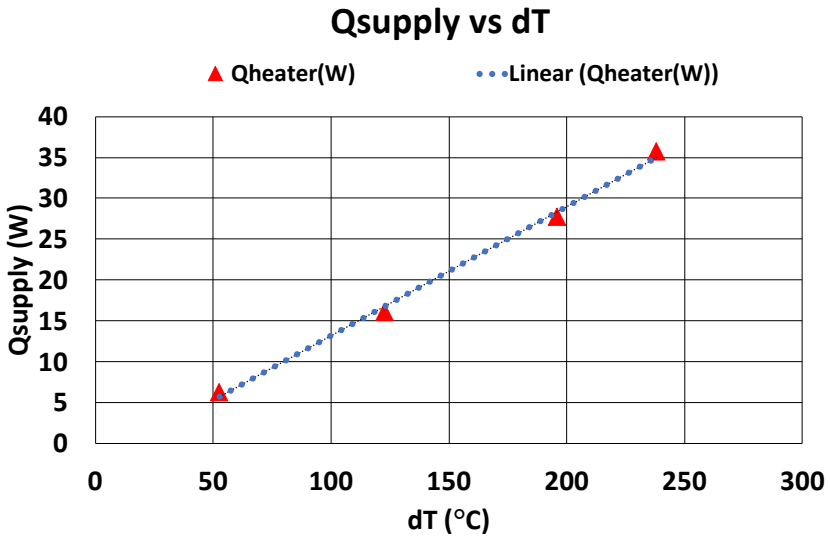

Fig. 2: 4pt Heat Loss Test

Pin Fin Array Geometry

- Pin fin arrays are often defined by the diameter of the pins along with the height, span-wise, and stream-wise distances between the pins to determine the array layout.
- The geometry was adopted from a matching array from Ames et al, eg [2005].
  - This was important so an experimental data set could aid in verifying the integrity of the simulation.
- The final test section was defined by a D = 2mm and confined to a staggered 7 x 14 pin array.

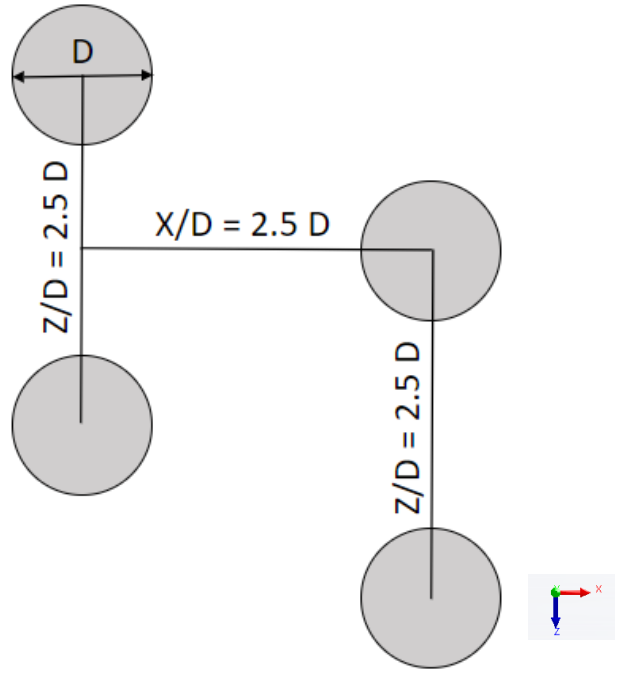

Pin fin array definition for the numerical model.

Real Gas Modeling - Thermophysical Properties

- Properties can vary significantly across sCO_2 thermophysical ranges.
- Importance to have adequate resolution of properties to represent fluid behavior.
- Common practice is using compressor exit for cooling where properties may vary.
- The red box indicates the testing range of the experiment and numerical setup.

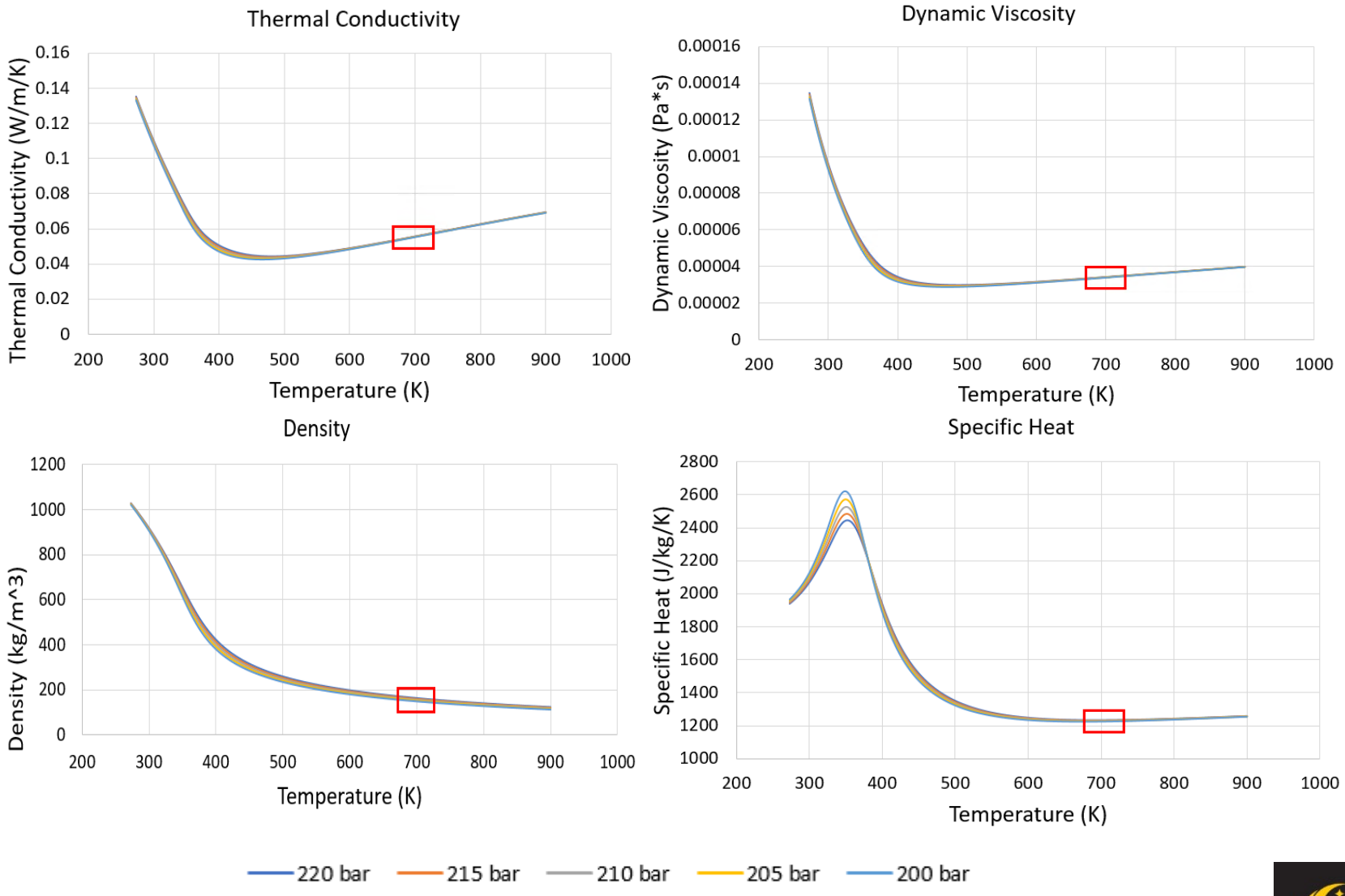

Carbon dioxide properties for various isobars. [Khadse 2020]

Real Gas Modeling – Test Parameters

- Real gas properties were modeled using user defined equations of state for both fluids.
  - Properties shown for sCO_2 at 200 bar
- Tables were generated using CoolProp [10], an open-source version of REFPROP, for all thermophysical properties for each fluid within a specified range of temperature and pressure.

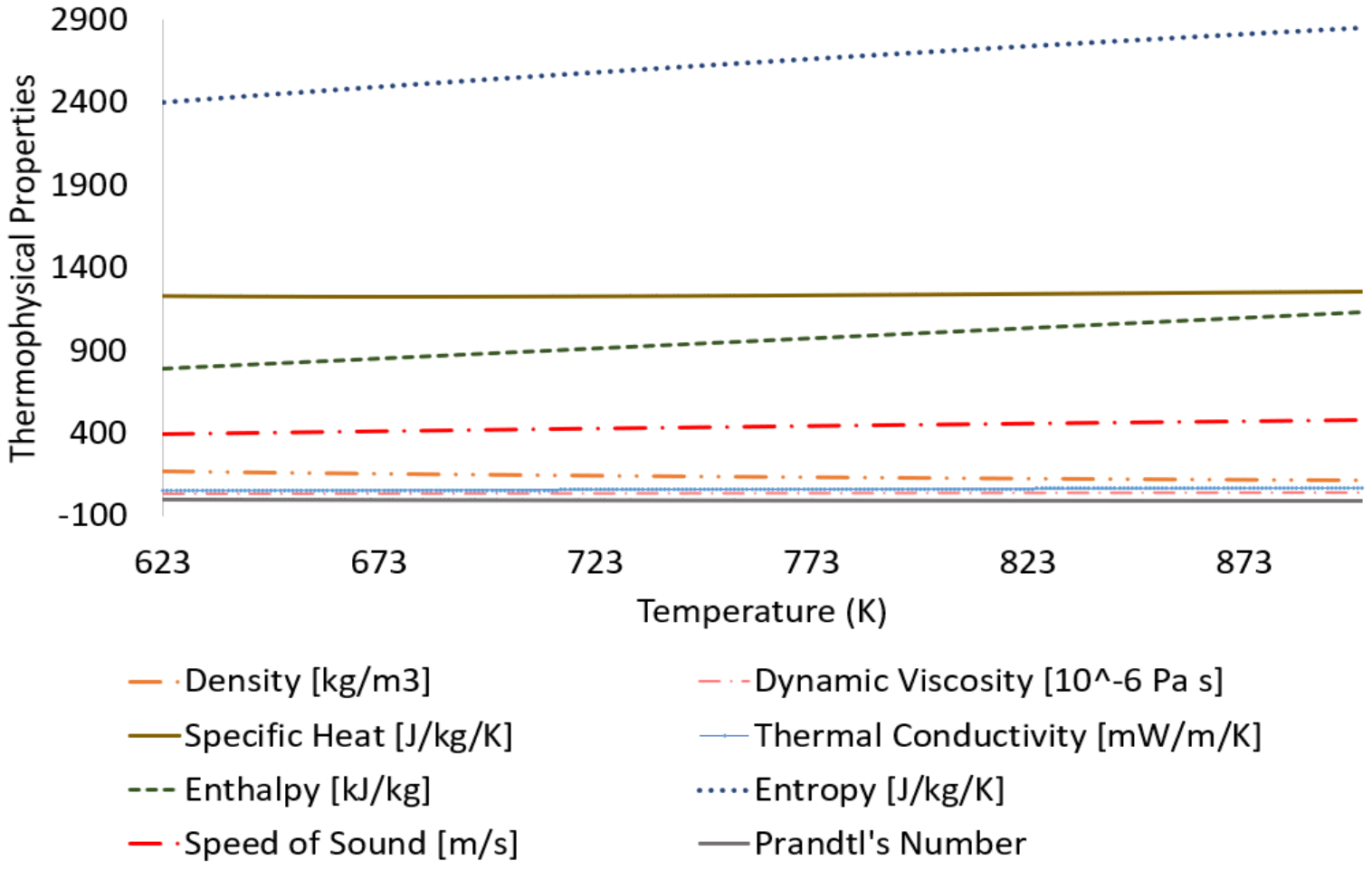

CFD Investigation

- Matching CFD was ran in parallel to the experiments to gain a more in depth understanding.
- First the extrapolated post processing method was compared to a direct measurment method in CFD.
- It showed the extrapolated wall temperature method brought us closer to the correlation trends, but still underpredicted.
- The CFD did verify our confidence in the first two points, and that the 66000 Reynolds number case was an outlier.

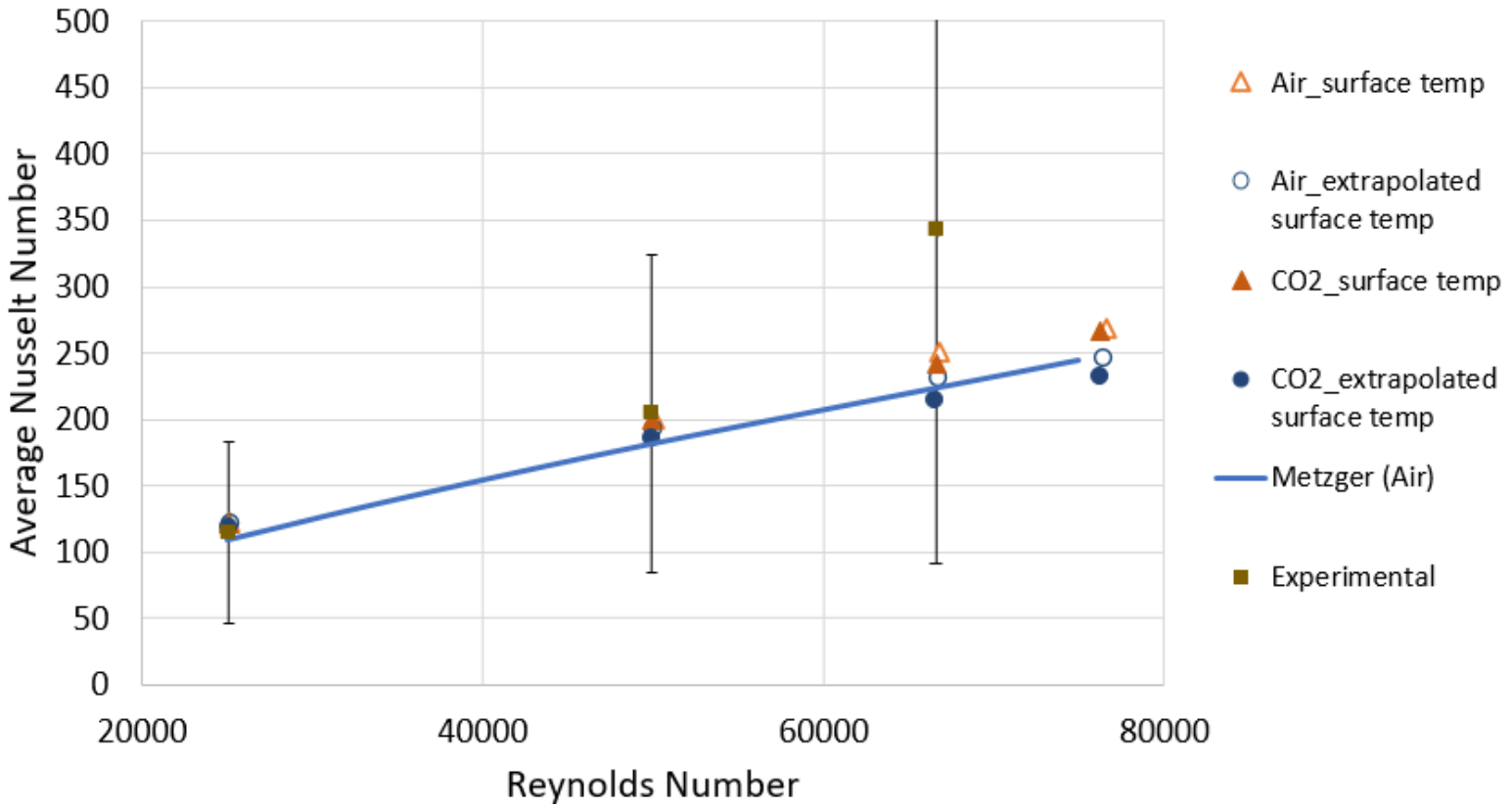

CFD Investigation

- CFD was used to compare the experimental and row-averaged post processing methods.
- Row averaging provided results that were closer to existing correlations and air validation, but this method wasn't feasible in the experimental scope.
- Without the ability for imaging in the high temp and pressure loop, like we can in our near critical loop, row averaged data would have had to be calculated using several thermocouples per row, which wasn't achievable inside the carbon steel pressure vessel.

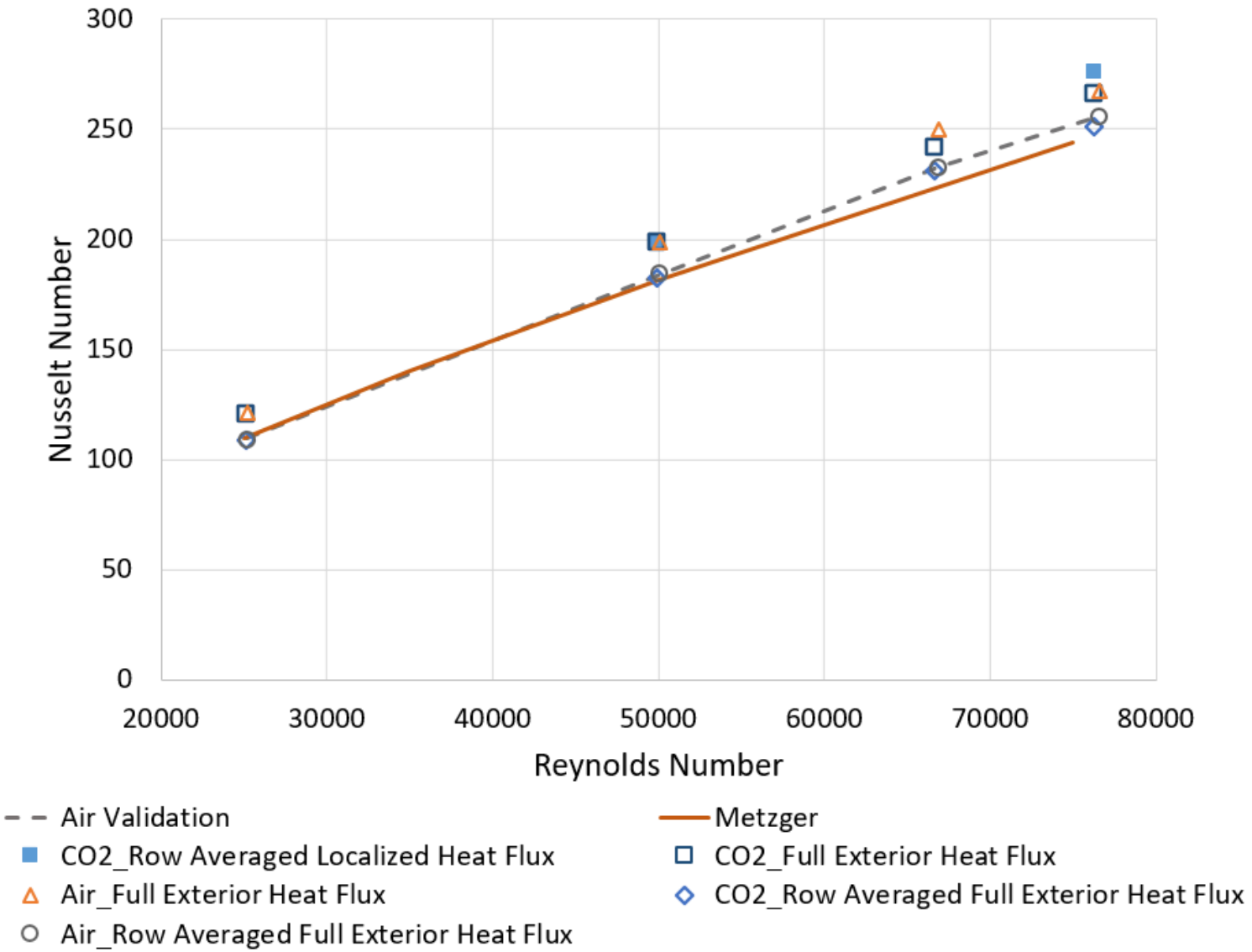

Disclaimer

- This report was prepared as an account of work sponsored by an agency of the United States Government. Neither the United States Government nor any agency thereof, nor any of their employees, makes any warranty, express or implied, or assumes any legal liability or responsibility for the accuracy, completeness, or usefulness of any information, apparatus, product, or process disclosed, or represents that its use would not infringe privately owned rights. Reference herein to any specific commercial product, process, or service by trade name, trademark, manufacturer, or otherwise does not necessarily constitute or imply its endorsement, recommendation, or favoring by the United States Government or any agency thereof. The views and opinions of authors expressed herein do not necessarily state or reflect those of the United States Government or any agency thereof.

References

- [White 2021] White, M. T., Bianchi, G., Chai, L., Tassou, S. A., and Sayma, A. I., 2021. “Review of supercritical co2 technologies and systems for power generation”. Applied Thermal Engineering, 185, p. 116447.
- [Ahn 2015] Ahn, Y., Bae, S. J., Kim, M., Cho, S. K., Baik, S., Lee, J. I., and Cha, J. E., 2015. “Review of supercritical co2 power cycle technology and current status of research and development”. Nuclear Engineering and Technology, 47(6) pp. 647–661.3 Copyright © 2022 by ASME
- [Crespi 2017] Crespi, F., Gavagnin, G., S´anchez, D., and Mart´ınez, G. S., 2017. “Supercritical carbon dioxide cycles for power generation: A review”. Applied Energy, 195, pp. 152–183.
- [Moore 2019] Moore, J. “Development of a high-efficiency hot gas turboexpander and low-cost heat exchangers for optimized csp supercritical co2 operation”
- [Allam 2016] Allam, R., Martin, S., Forrest, B., Fetvedt, J., Lu, X., Freed, D., Brown, G. W., Sasaki, T., Itoh, M., and Manning, J., 2017. “Demonstration of the allam cycle: An update on the development status of a high efficiency supercritical carbon dioxide power process employing full carbon capture”. Energy Procedia, 114, pp. 5948–5966. 13th International Conference on Greenhouse Gas Control Technologies, GHGT-13, 14-18 November 2016, Lausanne, Switzerland.
- [Lariviere 2021] Lariviere, B., Marion, J., Macadam, S., McDowell, M., Lesemann, M., McClung, A., and Mortzheim, J., 2021. “sco2 power cycle development and step demo pilot project”. 4th European sCO2 Conference for Energy Systems: March 23-24, 2021, Online Conference, Mar, p. 352–362.
- [Marion 2020] Marion, J., Lariviere, B., McClung, A., Mortzheim, J., and Ames, R., 2020. “The STEP 10 MWe sCO2 Pilot Demonstration Status Update”. Vol. Volume 11: Structures and Dynamics: Structural Mechanics, Vibration, and Damping; Supercritical CO2 of Turbo Expo: Power for Land, Sea, and Air. V011T31A002.
- [Otto 2019] Otto, M., 2019. “IMPROVING TURBINE PERFORMANCE: A CONTRIBUTION TO THE UNDERSTANDING OF HEAT TRANSFER AND VORTICAL STRUCTURES IN STAGGERED PIN FIN ARRAYS”. PhD Dissertation, University of Central Florida.
- [Khadse 2020] Khadse, A., 2020. "Supercritical CO2 Heat Transfer Study Near Critical Point in a Heated Circular Pipe". Electronic Theses and Dissertations, 2020-. 73. https://stars.library.ucf.edu/etd2020/73

References

- [Chyu 1990] Chyu, M. K., 1990. “Heat Transfer and Pressure Drop for Short Pin-Fin Arrays With Pin-Endwall Fillet”. Journal of Heat Transfer, 112(4), 11, pp. 926–932.
- [Metzger 1982] Metzger, D. E., and Haley, S. W., 1982. “Heat Transfer Experiments and Flow Visualization for Arrays of Short Pin Fins”. Vol. Volume 4: Heat Transfer; Electric Power of Turbo Expo: Power for Land, Sea, and Air. V004T09A007.
- [VanFossen 1982] VanFossen, G. J., 1982. “Heat-Transfer Coefficients for Staggered Arrays of Short Pin Fins”. Journal of Engineering for Power, 104(2), 04, pp. 268–274.
- [Viskanta 1993] Viskanta, R., 1993, “Heat Transfer to Impinging Isothermal Gas and Flame Jets, ” Exp,” Exp. Therm. Fluid Sci, 6(2), pp. 111–134
- [Bradbury 1965] Bradbury, L. J. S., 1965, “The Structure of a Self-Preserving Turbulent Plane Jet,” J. Fluid Mech., 23(01), p. 31.
- [Hrycak 1981] Hrycak, P., 1981, Heat Transfer From Impinging Jets A Literature Review, Air Force Wright Aeronautical Laboratories, Wright-Patterson AFB OH.
- [Huang 1963] Huang, G. C., 1963, “Investigations of Heat-Transfer Coefficients for Air Flow through Round Jets Impinging Normal to a Heat-Transfer Surface,” J. Heat Transfer, 85(3), pp. 237–243.
- [Martin 1977] Martin, H., 1977, “Heat and Mass Transfer between Impinging Gas Jets and Solid Surfaces,” *Advances in Heat Transfer*, Elsevier, pp. 1–60.
- [Huang 1994] Huang, L., and El-Genk, M. S., 1994, “Heat Transfer of an Impinging Jet on a Flat Surface,” Int. J. Heat Mass Transf., 37(13), pp. 1915–1923.
- [Sagot 2008] Sagot, B., Antonini, G., Christgen, A., and Buron, F., 2008, “Jet Impingement Heat Transfer on a Flat Plate at a Constant Wall Temperature,” Int. J. Therm. Sci., 47(12), pp. 1610–1619.
- [Goldstein 1986] Goldstein, R. J., Behbahani, A. I., and Heppelmann, K. K., 1986, “Streamwise Distribution of the Recovery Factor and the Local Heat Transfer Coefficient to an Impinging Circular Air Jet,” Int. J. Heat Mass Transf., 29(8), pp. 1227–1235.
- [Ames 2007] Ames, F. E., Nordquist, C. A., and Klennert, L. A., 2007. “Endwall Heat Transfer Measurements in a Staggered Pin Fin Array With an Adiabatic Pin”. Vol. Volume 4: Turbo Expo 2007, Parts A and B of Turbo Expo: Power for Land, Sea, and Air, pp. 423–432.
- [Ames 2005] Ames, F. E., Dvorak, L. A., and Morrow, M. J., 2005. “Turbulent Augmentation of Internal Convection Over Pins in Staggered-Pin Fin Arrays ”. Journal of Turbomachinery, 127(1), 02, pp. 183–190

References

- [Lardeau 2016] Lardeau, S., and Billard, F. development of an elliptic-blending lag model for industrial applications.
- [Bell 2014] Bell, I. H., Wronski, J., Quoilin, S., and Lemort, V., 2014. “Pure and pseudo-pure fluid thermophysical property evaluation and the open-source thermophysical property library coolprop”. Industrial & Engineering Chemistry Research, 53(6), pp. 2498–2508.
- [Otto 2019] Otto, M., Hodges, J., Gupta, G., and Kapat, J. S., 2019. “Vortical Structures in Pin Fin Arrays for Turbine Cooling Applications”. Vol. Volume 5A: Heat Transfer of Turbo Expo: Power for Land, Sea, and Air. V05AT16A003.
- [Manceau 2002] Manceau, R., and Hanjalic, K., 2002. “Elliptic blending model: A new near-wall reynolds-stress turbulence closure”. Physics of Fluids, 14, pp. 744–754.
- [Delibra 2009] Delibra, G., Borello, D., Hanjali´c, K., and Rispoli, F., 2009. “Urans of flow and endwall heat transfer in a pinned passage relevant to gas-turbine blade cooling”. International Journal of Heat and Fluid Flow, 30(3), pp. 549–560. The Seventh International Symposium on Engineering Turbulence Modelling and Measurements, ETMM7.
- [Khadse 2019] Khadse, A., Curbelo, A., and Kapat, J. S., 2019. “Numerical Study of Radiation Heat Transfer for a Supercritical CO2 Turbine Linear Cascade”. Vol. Volume 9: Oil and Gas Applications; Supercritical CO2 Power Cycles; Wind Energy of Turbo Expo: Power for Land, Sea, and Air. V009T38A026.
- [Allam 2016] Allam, R., Martin, S., Forrest, B., Fetvedt, J., Lu, X., Freed, D., Brown, G. W., Sasaki, T., Itoh, M., and Manning, J., 2017. “Demonstration of the allam cycle: An update on the development status of a high efficiency supercritical carbon dioxide power process employing full carbon capture”. Energy Procedia, 114, pp. 5948–5966. 13th International Conference on Greenhouse Gas Control Technologies, GHGT-13, 14-18 November 2016, Lausanne, Switzerland.
- [Moore 2023] Moore, J., Neveu, J., Bensmiller, J., Replogle, C., Lin, J., Fetvedt, J., Cormier, I., Kapat, J., Fernandez, E., Paniagua, G., 2023. ‘DEVELOPMENT OF A 300 MWE UTILITY SCALE OXY-FUEL SCO2 TURBINE”. Proceedings of ASME Turbo Expo 2023, *To Be Published.*
- [Wardell 2022] Wardell, RJ, Otto, M, Smith, M, Fernandez, E, & Kapat, J. "A Numerical Study on Conjugate Heat Transfer of Supercritical Carbon Dioxide Cooling in a Staggered Pin Fin Structure." Proceedings of the ASME Turbo Expo 2022: Turbomachinery Technical Conference and Exposition. Volume 6B: Heat Transfer — General Interest/Additive Manufacturing Impacts on Heat Transfer; Internal Air Systems; Internal Cooling. Rotterdam, Netherlands. June 13–17, 2022. V06BT15A015. ASME. https://doi.org/10.1115/GT2022-82044

Thank you for your attention!

Emmanuel Gabriel-Ohanu
emmanuel.gabriel-ohanu@ucf.edu

University of Central Florida
Center for Advanced Turbomachinery and Energy Research
Laboratory for Cycle Innovation and Optimization